



HAL
open science

Spatial distribution of Rare Earth Elements in a transnational watershed: The case of the Danube River

Pauline Louis, Davide A.L. Vignati, Steve Pontvianne, Marie-Noëlle Pons

► To cite this version:

Pauline Louis, Davide A.L. Vignati, Steve Pontvianne, Marie-Noëlle Pons. Spatial distribution of Rare Earth Elements in a transnational watershed: The case of the Danube River. *Science of the Total Environment*, 2023, pp.164368. 10.1016/j.scitotenv.2023.164368 . hal-04108614

HAL Id: hal-04108614

<https://hal.science/hal-04108614>

Submitted on 27 May 2023

HAL is a multi-disciplinary open access archive for the deposit and dissemination of scientific research documents, whether they are published or not. The documents may come from teaching and research institutions in France or abroad, or from public or private research centers.

L'archive ouverte pluridisciplinaire **HAL**, est destinée au dépôt et à la diffusion de documents scientifiques de niveau recherche, publiés ou non, émanant des établissements d'enseignement et de recherche français ou étrangers, des laboratoires publics ou privés.

Spatial distribution of Rare Earth Elements in a transnational watershed: the case of the Danube River

Pauline LOUIS¹, Davide A.L. VIGNATI², Steve PONTVIANNE¹, Marie-Noëlle PONS^{1,3*}

1 Université de Lorraine, CNRS, LRGP, F-54000 Nancy, France

2 Université de Lorraine, CNRS, LIEC, F-57000 Metz, France

3 LTSER-Zone Atelier du Bassin de la Moselle, LRGP, 54000, Nancy, France

*Corresponding author: marie-noelle.pons@univ-lorraine.fr

Accepted version, may contain errors corrected later during production

Abstract

The distribution of Rare Earth Elements was investigated along the Danube River (from its sources in Germany to its delta in Romania/Ukraine) and in some of its tributaries for the first time during the fourth Joint Danube Survey (JDS4) in 2019. The negative Ce anomaly and the La/Lu ratio tend to decrease between Ulm (Germany) and the Black Sea, indicating an increasing trend of the anthropogenic influence as the Danube River runs toward the sea. This diffuse influence is also attested by the slow spatial variation of classical pollution parameters such as dissolved organic carbon (amount and optical characteristics) and nitrates. A strong gadolinium (Gd) anomaly (between 6 and 10), due to the release of anthropogenic Gd, was detected starting 10 km downstream the sources of the Breg River and the Brigach River, whose junction forms the Danube River. The anomaly remains larger than 10 until the Danube River leaves Croatia at Ilok. The anomaly pattern is related to the difference in the use of magnetic resonance imaging (MRI) in the countries sharing the Danube River watershed. The estimated annual flux of anthropogenic gadolinium in the Black Sea is 0.9 ton/year. An Ytterbium anomaly was detected in stations close to the delta and needs further investigation.

Keywords: Anomaly; Gadolinium; Magnetic resonance imaging; Ytterbium

1. Introduction

Rare Earth Elements (REEs), i.e. the fifteen lanthanides (from Lanthanum to Lutetium) to which Yttrium and Scandium are often associated, are increasingly present in our modern life: Y, La, Ce, Eu, Gd, and Tb in fluorescent lamps (Hobohm et al., 2016), Ce in batteries (Porvali et al., 2020), Nd, Pr and Dy in permanent magnets, La in catalysts (Kulaksız and Bau, 2011a), Ce in diesel fuel additives (Dale et al., 2017) are some examples. Anthropogenic uses of REE can both increase their concentrations above natural background levels and alter their natural distribution pattern by introducing anomalies in REE profiles. While the solid waste that may result from their use can be collected and potentially reprocessed (Hobohm et al., 2016; Yang et al., 2017; Porvali et al. 2020; Becci et al., 2021), the same is not true for REEs used in the medical field, in particular in contrast agents. These include Gd-based contrast agents (GBCAs), used in Magnetic Resonance Imaging (MRI) examinations. GBCAs are eliminated through the urine and are therefore found in urban wastewater. These complexes are non-biodegradable and pass through wastewater treatment facilities to be released into aquatic environments. Since the first evidence (Bau and Dulski, 1996), the presence of Gd has been detected in aquatic ecosystems in many countries, even when they do not have MRI facilities. Table S1 provides data extracted from literature about Gd concentrations in non-saline surface waters around the world. It is difficult to calculate an average value as the data were obtained over 25 years in different hydrological conditions, in pristine waters as well as in highly urbanized areas. The highest value was measured (492 ng/L) in Postdam (Berlin/Brandenburg Metropolitan Area) by Kulaksız and Bau (2011b).

Although Gd is probably the most documented REE as a micropollutant of increasing concern, anthropogenic La has been detected in the Rhine River in Germany (Kulaksız and Bau, 2011a).

In water samples (Kulaksız and Bau, 2013) ~~as well as in shells (Valdés-Vilchis et al., 2021)~~, samarium positive anomalies have been related to petrochemical industries, where Sm-based catalysts are used. Furthermore, the industrial activities related to the extraction and purification of REEs as well as REE-based products manufacturing can release REEs in aquatic ecosystems. According to Chen et al. (2021), contamination by REEs of the Qinhui River in China might be related to electronic waste recycling and permanent magnet industries. In Dingnan County (China) heavy contamination of soil and water has been recorded close to a REEs mine (Liu et al., 2019). Mining activities not focusing directly to REEs can also be the source of contamination by these elements, as shown by Khan et al. (2016) in a former tin mining area. Runoff from agricultural fields where municipal sludge (Kaegi et al., 2021) and/or chemical fertilizers (Hu et al., 2004; Turra, 2018) have been applied can participate also to surface waters pollution by REEs. Urban runoff, contaminated by particulate pollution related to coal burning and transport activities, is also a contributor of La and Ce discharges in surface water (Shajib et al., 2020).

Once anthropogenic REEs are detected in surface water, there is a risk of transfer to drinking water. Bank filtration is used in many countries for drinking water production and its efficiency as a barrier against transfer of pharmaceutical residues has been questioned (Kondor et al., 2020). As early as 2009, Gd has been detected as a micropollutant in tap water in Berlin (Kulaksız and Bau, 2011b), with a rapid increase over a few years (Tepe et al., 2014). Bank filtration is not the only way to get anthropogenic Gd into tap water: karst aquifers can be easily contaminated as shown by Rabiet et al. (2009) in the Hérault watershed (France) and Boester and Rüde (2020) in Bavaria. Recently anthropogenic Gd has been reported in four tap waters in China, in the district of Guiyang (Han et al., 2021). If Gd-related health risks were thought to be minimal when GBCAs started to be used in the 1980s, more recent data indicate

possible retention in different human organs such as kidney (Fraum et al., 2017), brain (Chazot et al., 2020) or bones (Veiga et al., 2020). Thomsen (2017) has suggested monitoring more closely Gd as risks associated with tap water are not well known. Accumulation of REE has been detected in many aquatic organisms (such as crabs (Lavezzo et al., 2020) and bivalves shells (Merschel and Bau, 2015; Le Goff et al., 2019, Mouchi et al., 2020; Valdés-Vilchis et al., 2021) with the Gd anomaly linked to anthropogenic uses remaining detectable in bivalves (Pereto et al. 2020) and fish (Lortholarie et al., 2020). However, REEs seem to undergo biodilution along the food chain (Amyot et al., 2017; Santos et al, 2023) and the possible risks associated to their dietary uptake remain to be elucidated. Recently, Souza et al. (2021) discussed the evidence of high bioaccessibility of gadolinium-contrast agents after ingestion of Gd-contaminated tap water.

If anthropogenic REEs have been detected in different aquatic ecosystems, in particular in rivers, the number of samples collected is often limited to a couple as it can be seen in Table S1 (Supplementary Information section). It has to be recognized that sampling in watersheds of large rivers requires sophisticated logistics: Zhang et al. (1998) could only investigate the Yangtze River lower section (eight stations on about 1,000 km of a 6,300 km-long river) downstream of the city of Wuhan. Ma and Wang (2023) managed to sample 15 stations on tributaries of the complex Pearl River delta. In such cases, it is difficult to relate the REE concentration to the watershed characteristics and disentangle the actual contributions due to anthropogenic pressures from geological factors (Louis et al., 2020).

The fourth Joint Danube Survey (JDS4), which took place in summer 2019, was an extraordinary opportunity to monitor for the first time the REEs along the Danube River and in some of its tributaries. The Danube River watershed is the second largest in Europe with a

surface of about 800,000 km² and is shared by nineteen countries, making it the most international river basin in the world, with a total population of 81 million inhabitants. Organized by the ICPDR (International Commission for the Protection of the Danube River) Monitoring and Assessment Expert Group, JDS4 made possible the sampling in twelve countries over a period of about one month (JDS4, 2021).

The purpose of the present study is to report for the first time the spatial distribution of REE concentrations in the Danube watershed and put this distribution in relation with those of other elements (alkaline earth metals, major ions (i.e., sulfates, chlorides and nitrates)), dissolved organic carbon (DOC) concentration and typology and the population living in this transnational watershed.

2. Materials and methods

2.1. Sampling

The full list of all sample locations, with their codes, is given in the Supplementary Information section (Table S2 for the Danube River and Table S3 for its tributaries). Sampling upstream from Ulm took place July 3rd (between Neu Ulm and Donaueschingen) and July 4th 2019 (along the Breg River and the Brigach River between Donaueschingen and the river sources) (Figure 1). Samples (n = 35) were grabbed from bridges (except at the sources), 5 cm below the surface using a bailer made of high-density polyethylene (PEHD) (SDEC, Reignac-sur-Indre, France). Two tributaries were also sampled (Eisenbach River and Iller River) and two drinking water samples were collected in Donaueschingen and Ulm. The samples were transferred into clean 250 mL HDPE (High-Density PolyEthylene) bottles and kept in a coolbox in the dark until the arrival in the lab. They were then stored at 4°C in the dark pending treatment within 24hrs.

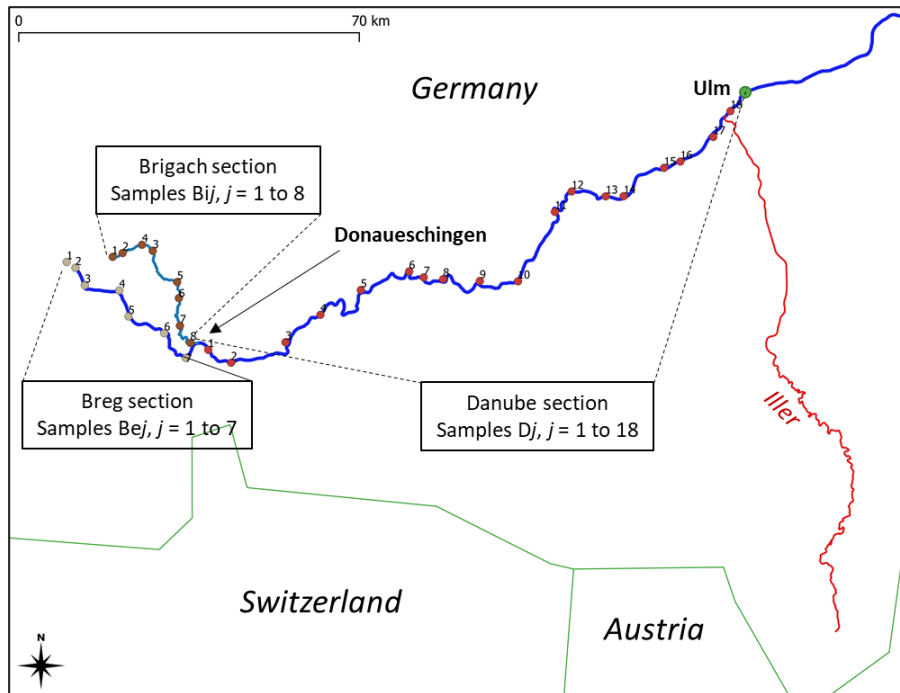


Figure 1: Sampling sites along the Danube River between Ulm and Donaueschingen (samples D01 to D18), the Brigach River (samples Bi1 to Bi8) and the Breg River (Be1 to Be7).

Sampling downstream from Neu Ulm took place in mid-July, 2019, within the framework of the JDS4 (Figure 2). The sampling team in each country had previously received clean 500 mL HDPE bottles. Fifty-one samples were grabbed along the Danube and some of its tributaries from the banks or from the middle of the river. Groundwater samples were also collected in wells recharged with Danube water through bank filtration in Austria, Slovakia, Hungary, Croatia, Serbia, Romania and Bulgaria (Figure 2).

All samples were stored in a coolbox in the dark and transferred to the Environmental Institute (Kos, Slovakia) prior to their overnight shipment to France where they underwent pre-treatment within one day.

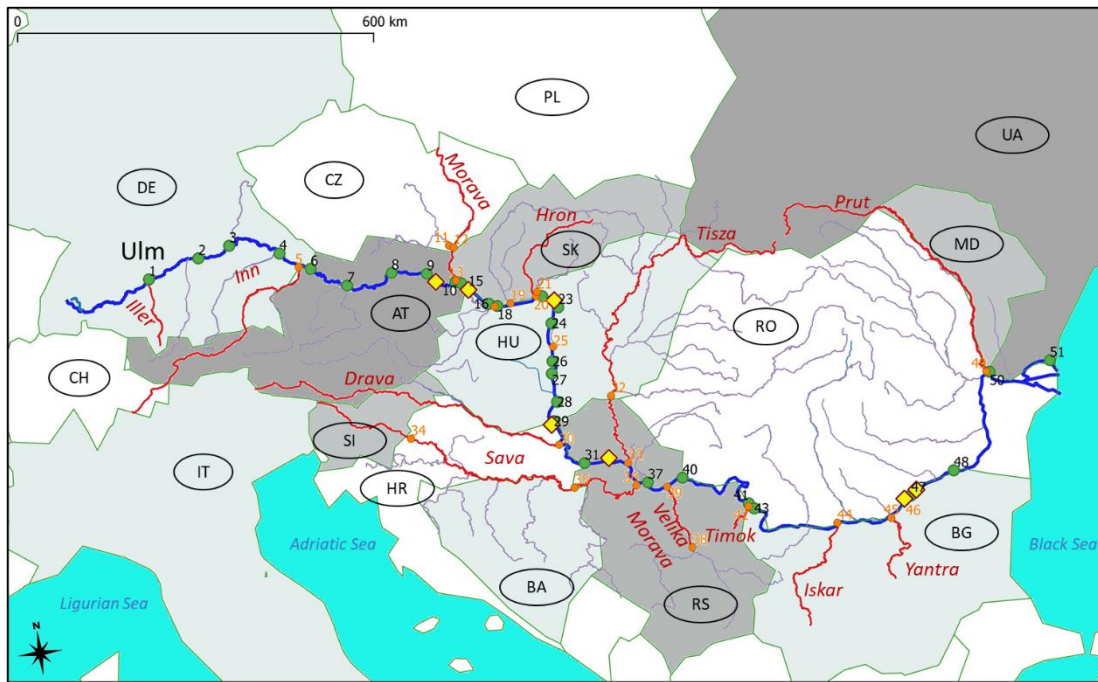


Figure 2: Sampling sites along the Danube River between Ulm and the Black Sea (green dots) and some of its tributaries (orange dots) and groundwater samples (yellow diamonds).

2.2 Analytical methods

2.2.1 Sample filtration and ancillary parameters

Samples were filtered through regenerated cellulose syringe filters (Phenomenex®) with 0.45 μm nominal pore size. Only the filterable fraction, which consists of dissolved ions and colloids $< 0.45 \mu\text{m}$, is considered in the present paper. Aliquots (50 mL for REEs, 10 mL for major elements) of the filterable fraction were acidified immediately after filtration with ultrapure HNO_3 (at 1% v/v, acid class “Optima” for REEs and at 2% v/v, acid class “Trace Metal” for major cations). Other sample aliquots (80 mL) were preserved at 4 °C without acidification for measurements of dissolved organic and inorganic carbon (DOC and DIC), total nitrogen (TN), major anions and characterization of the dissolved organic matter (DOM) by optical methods (section 2.2.3). DOC and DIC were measured with a Shimadzu TOC VCHS combined with a TNM-1 module for TN determination. Major anions (Cl^- , SO_4^{2-} , NO_3^-) were determined by ion

chromatography (Thermo Scientific Dionex iCS 3000) and major cations (Mg, Na, K, and Ca) by inductively coupled plasma atomic emission (ICP AES) (Thermo Scientific iCAP 6300 Duo).

2.2.2. REEs analysis

REEs were determined using Inductively Coupled Plasma Mass Spectrometry (ICP-MS) (Thermo Scientific iCAPQ+prepFast) without preconcentration. Re and Rh at 50 ppb were used as online internal standards. The instrument was tuned for oxide and doubly charged ion formation, and interference corrections for oxide and hydroxide were applied when necessary. The analytical error was below 5%. The quantification limit, calculated as 10 times the standard deviation of replicated blank measurements, was 1 ng/L for all REEs. The filtration blank results (n = 15) were always below detection limits. SLRS-6 reference water was used to control the ICP-MS accuracy and reproducibility (Yeghicheyan et al., 2019) (Table S3).

The REEs concentrations were normalized by the Post Archean Australian Shale (PAAS) (McLennan, 1989; Rétif et al., 2023). The Ce and Gd anomalies were calculated using Eq (1) and Eq(2) (Hissler et al., 2015), respectively.

$$\text{Ce/Ce}^* = \text{Ce}_{\text{PAAS}} / (0.5 \times \text{La}_{\text{PAAS}} + 0.5 \times \text{Pr}_{\text{PAAS}}) \quad (1)$$

$$\text{Gd/Gd}^* = \text{Gd}_{\text{PAAS}} / (0.4 \times \text{Nd}_{\text{PAAS}} + 0.6 \times \text{Dy}_{\text{PAAS}}) \quad (2)$$

where X is the measured concentration in samples, X* the calculated geogenic concentration, and X_{PAAS} the concentration normalized by the PAAS. Finally the anthropogenic Gd concentration was deduced using Eq(3):

$$\text{Gd}_{\text{anth}} = \text{Gd} - \text{Gd}^* \quad (3)$$

It should be noticed that the calculation method used in the present study for the Gd anomaly tends to maximize the value of the Gd anomaly compared with other calculation methods (Louis et al., 2020; Rétif et al., 2023).

2.3. Optical methods

Synchronous fluorescence spectra (SF50) were collected on a Hitachi F-2500 fluorimeter equipped with a Xenon lamp, by using FL Solution 2.0 software and a 1 cm x 1 cm 3.5 mL quartz cuvette. The gap between excitation and emission was set at 50 nm. The 50 nm deviation provides information on both fluorescence due to protein-like substances (excitation at around 280 nm) (Baker et al., 2002) and humic substances (humic acids and fulvic acids; excitation between 300 nm and 400 nm) (Coble, 1996). Since the absorbance of the sample may interfere with fluorescence, the absorbance at 254 nm was checked for each sample. UV-vis spectra (200-600 nm) were collected on a Shimadzu UV-2600 spectrophotometer, using a 1 cm x 1 cm quartz 3.5 mL cuvette. Ultra-pure water was used for blanks.

As A_{254} was less than 0.1 cm^{-1} for 90% of the samples, the absorbance was considered low enough to record fluorescence directly, without any correction for the inner-filter effect. The SF50 spectra were collected at the natural pH of the samples. The blank was performed with ultra-pure water. The fluorescence intensities were expressed in Raman units (R.u.).

To extract quantitative information out of the SF50 spectra, a decomposition procedure was applied (Assaad et al., 2015). In this approach, the synchronous fluorescence spectrum of a single fluorophore is represented by a Gauss function (Eq (4)):

$$SF(\lambda) = F(b) \cdot \exp(-(\lambda - b)^2 / 2c^2) \quad (4)$$

where $F(b)$ is the pseudo-concentration of the fluorophore, b (in nm) its characteristic excitation wavelength, i.e. the wavelength where the maximal fluorescence is recorded and c a parameter related to the width of the Gauss function. Each SF50 spectrum was decomposed into five Gauss functions (i.e., distinct fluorophores groups) by deconvolution. With a 50 nm gap the water Raman scatter interferes with the fluorescence of the fluorophore with a characteristic excitation wavelength of 355 nm and the contribution of water to this fluorophore is further corrected for.

2.4. Databases

Maps were constructed using Qgis 3.16 (<https://www.qgis.org>). Shape files for the Danube River and its main tributaries were extracted from the WISE database (<https://www.eea.europa.eu/data-and-maps/data/wise-large-rivers-and-large-lakes>).

Brigach and Breg courses were obtained from the Baden-Württemberg Government (<https://rips-dienste.lubw.baden-wuerttemberg.de>).

The location and the capacity of the urban wastewater treatment plants along the Danube River and its (sub)tributaries were obtained from the dissemination platform of the Urban Waste Water Treatment Directive (UWWTD) (<https://uwwtd.eu/>) for the EU countries (2016 data) and from ICPDR for non-EU countries.

The 1:1,000,000 geological (GK1000) data of Germany were downloaded from the database of the federal Institute for Geosciences and Natural Resources (<https://www.bgr.bund.de>).

Ancillary data for DOC and nitrates were compared to the 2017 water quality data provided by ICPDR through the TransNational Monitoring Network (TNMN) scheme (https://www.icpdr.org/main/sites/default/files/nodes/documents/tnmn2017_annex_1.xls).

Flow rates in some specific stations were measured during the JDS4 and retrieved from the JDS4 database (<https://data.danubesurvey.org/jds4/>).

The Eurostat database provided the data about the number of MRI examinations in Europe (<https://data.europa.eu>). Complementary data for non-EU countries were extracted from the OECD Health Database (<https://www.oecd.org/els/health-systems/health-data.htm>).

The distances are established from the mouth at the Black Sea for the Danube River and from the confluence with the Danube River for its tributaries. The Danube River is divided into three main parts: the Upper Danube River refers to the river course between the sources and rkm 1789.5 (Klížská Nemá, Slovakia); the Middle Danube River to the river course between rkm 1789.5 and rkm 943 (Turnu Severin, Romania); the Lower Danube River to the river course between rkm 943 and the Black Sea (https://www.icpdr.org/flowpaper/viewer/default/files/roof_report_2004_annexes.pdf).

3. Results and discussion

3.1. Physical-chemical parameters

This section summarizes the main characteristics of the surface water of the Danube, and particularly those related to dissolved organic matter (DOM) and nitrates which can provide information on the global anthropogenic pressure on the river basin.

In their upper parts, the Brigach River and the Breg River are flowing on silica-rich rocks (granite, sandstone). Their concentrations in alkaline minerals (calcium, magnesium, potassium and sodium) increase gradually moving downstream where they are leaching Triassic and Jurassic rocks (i.e. limestone, marlstone) (Figure S1 and Table S5). At Ulm, the

Danube River meets the Iller River, its first large tributary (Figure 3). This alpine river average flowrate at the confluence is larger than the Danube River average flowrate ($70 \text{ m}^3/\text{s}$ versus $53 \text{ m}^3/\text{s}$), which causes a strong dilution. This dilution (Figure S2) is further accentuated at the junction with the Inn River, a large alpine tributary of low mineral content (Table S5) whose discharge flowrate is similar to that of the Danube at their junction ($\approx 2200 \text{ rkm}$). The Inn River has its maximal flowrate in summer due to the snow melting in the Alpine upper part of its watershed (Figure S3). Its dilution effect is seen on the mineral content of the Danube waters (Figure S2). Downstream Passau, the calcium, magnesium and potassium concentrations are stable until the Danube reaches the Black Sea. The sodium concentration increases, which can be seen as a result of the discharge, in the aquatic environment, of urban wastewater containing detergent residues.

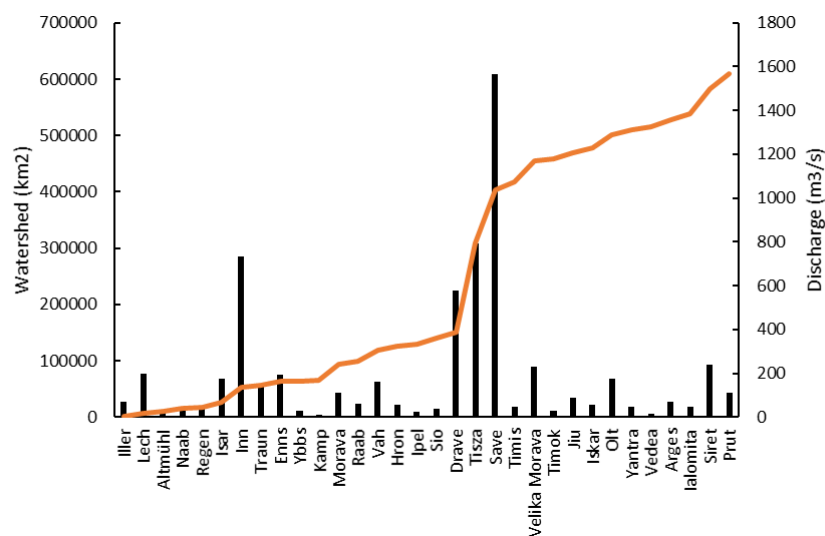


Figure 3: Danube River watershed area (in orange) as a function of the received tributaries (average annual discharge in black).

DOC is higher in the samples collected upstream Ulm, in particular in the waters of the Brigach River and of the Danube River, than downstream Ulm (average of 3.1 mg/L and 2.0 mg/L respectively) (Figure 4). The Inn River carries very little DOC (0.5 mg/L in Passau-Ingling) (Table

S4). DOC does not vary much in the middle section of the Danube River (average of 1.7 mg/L). Large inflows from the tributaries (up to 7.5 mg/L for Morava River) are quickly diluted: the Morava River discharge rate is only 6% of the Danube River at their junction. In the Lower Danube, DOC increases (average 2.8 mg/L), which seems to be controlled by inflows from tributaries with less dilution effects than upstream. This increase in DOC in the Lower Danube was also highlighted during the JDS3 campaign (Joint Danube Survey 3, 2015).

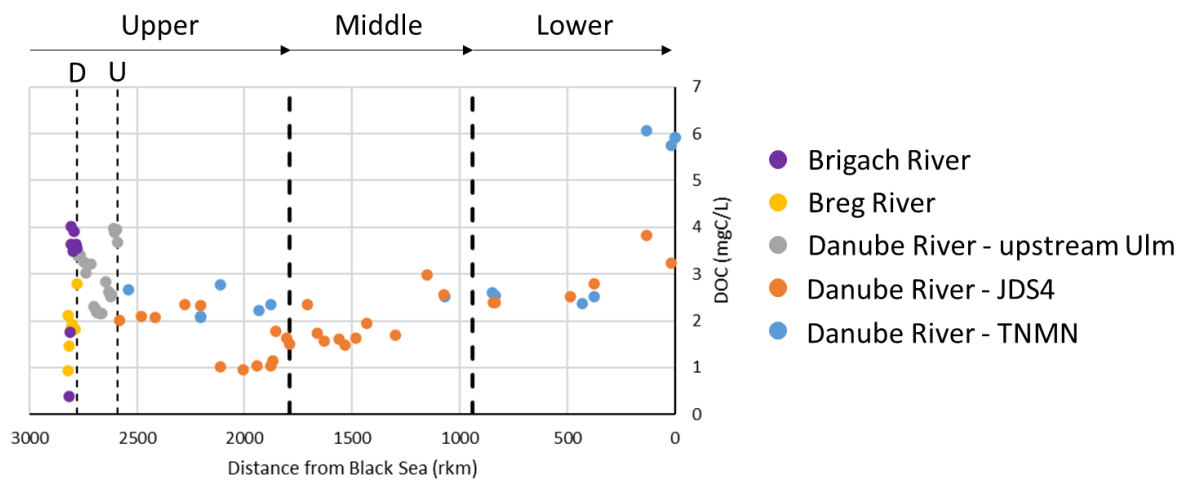


Figure 4: Dissolved organic carbon (DOC) along the Danube River. D = Donaueschingen, U = Ulm. JDS4: Joint Danube survey 4 (present study), TNMN, Trans-National Monitoring Network (2017).

Synchronous fluorescence spectra and their deconvolution provide further insight into the nature of DOM (Figure 5). Protein-type fluorophores are linked to biological reactions in water but also to the runoff of biological substances from the watershed and the discharge of raw sewage or insufficiently treated urban wastewater. Their fluorescence is largely due to the presence of the indole group which is present in tryptophan (an essential amino acid for humans, which is produced only by microorganisms and plants), in auxins (plant hormones) and in acids bound to urine (such as, for example, 5-hydroxy-indolyacetic acid, a metabolite

of serotonin). Other fluorescent substances that can be found in the same spectral region as tryptophan in the SF50 spectra are threonine ($\lambda_{exc} \approx 280$ nm), another essential amino acid for humans, and tyrosine ($\lambda_{exc} \approx 270$ nm), also an amino acid.

In the Danube watershed, the total pseudo-concentrations of fluorophores vary from 0.042 to 0.235 Raman units. These pseudo-concentrations are globally higher for the samples from the Brigach River and the Upper Danube River (0.065 to 0.235 Raman units). They decrease in the Median Basin (0.042 to 0.105 Raman units) before increasing after the confluence with the Timok (SW42-Tim) in the Lower Basin and the Delta (0.074 to 0.141 Raman units). The Eisenbach River, the Iller River and the Inn River carry little fluorescence. Other tributaries such as the Morava River, the Hron River, the Ipel River, the Tisza River and the Sava River bring a high quantity of fluorescent dissolved organic matter in the Upper and Middle sections of the Danube River Basin (0.114 to 0.208 Raman units). However, these contributions seem to disappear rapidly under the effects of dilution with the Danube River waters, as observed for the DOC values. In the Lower section of the Danube River basin and in its delta, the contribution of other tributaries (Iskar River, Yantra River, Russenski Lom River and Prut River) is also significant (0.103 to 0.211 Raman units) and seems less affected by dilution effects, as the fluorescence of the River Danube waters is higher downstream.

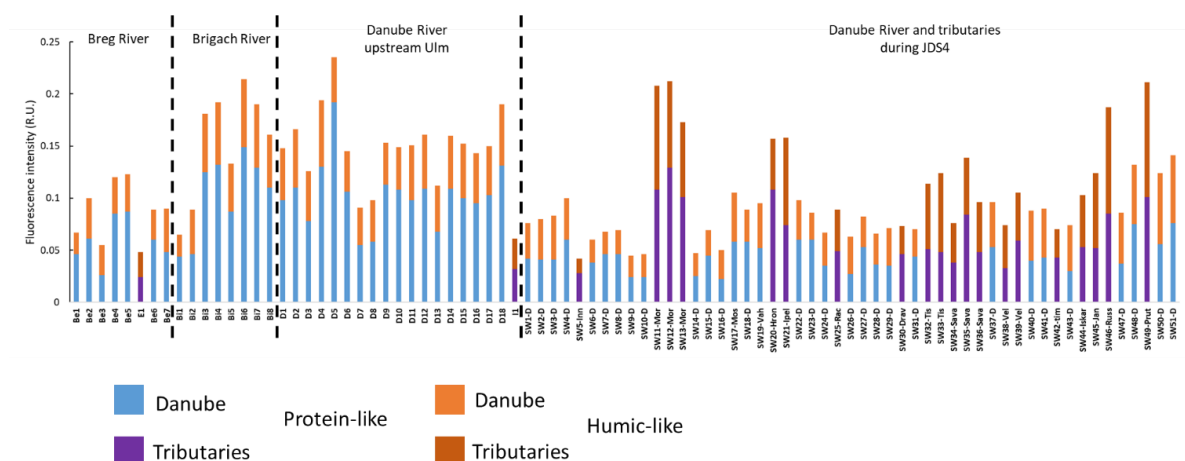


Figure 5: Protein-like and humic-like fluorescence in the Danube River watershed in July 2019.

In the Upper Basin, the fluorophores of the protein type (F (280) and F (310)) represent 47 to 82% of the total fluorescence, and the fluorophores of the humic-fulvic type (F (330), F (355), F (370)) 18 to 53%. In the Middle Basin, protein-type fluorophores represent 39 to 70% of the total fluorescence, and humic-fulvic-type fluorophores 30 to 61%. Finally, in the Lower Basin and in the delta, protein-type fluorophores represent 40 to 61% of the total fluorescence, and humic-fulvic-type fluorophores 39 to 60%. Downstream Ulm, there is no clear prevalence of protein-like or humic-fulvic-like DOM in the Danube River watershed, except for some tributaries (such as Morava River, Hron River, Ipel River, Prut River). The humic-fulvic-like DOM is partly of allochthonous origin (terrestrial origin resulting from the degradation of plants) of the DOM, due to soil leaching. An anthropogenic origin can also be assumed due to discharge of non-biodegradable pollution originating from wastewater treatment plants effluents. The DOM of the upstream part shows, by contrast, a rather autochthonous origin, resulting from the biological activity of algae or bacteria (the Danube being quite shallow upstream of Ulm, aquatic plants and algae development could be favored by facilitated photosynthesis), or treated wastewater discharged from WWTPs. The high population density, such as the one observed in Germany ($\approx 230 \text{ inh/km}^2$) combined with relatively small flowrates, especially in summer, induces low dilution rates of treated wastewater in the receiving bodies. The average yearly flowrates of the Brigach River and the Breg River at Donaueschingen are $3.3 \text{ m}^3/\text{s}$ and $5 \text{ m}^3/\text{s}$, respectively (<https://www.hvz.baden-wuerttemberg.de/>).

Nitrates can be introduced into aquatic systems via atmospheric emissions, fertilizer runoff and effluents from wastewater treatment plants. Nitrates are higher in the waters of the

Brigach River and in the samples from the Danube River between Donaueschingen and Ulm than in the samples from the JDS4 (Figure 6). Among the tributaries of the Danube, the Russenski Lom (Bulgaria) has the highest concentration (29.8 mgNO₃ / L), but its contribution disappears in the waters of the Danube with the effects of dilution. During the 2013 JDS3 campaign, Russenski Lom already showed the highest nitrate concentration (5.2 mg / L N-NO₃ or 23 mgNO₃ / L) (JDS3 report, 2015), and a decrease in the nitrate concentration was observed from upstream (Ulm, Germany) to downstream (delta) for the Danube River waters (from 14 to 3.9 mgNO₃ / L). The nitrate concentration is practically stable between rkm 2250 (junction with the Inn River (running down from the Aps mountains) and the delta. This means that the nitrate flux becomes larger as the Danube River flows toward the Black Sea.

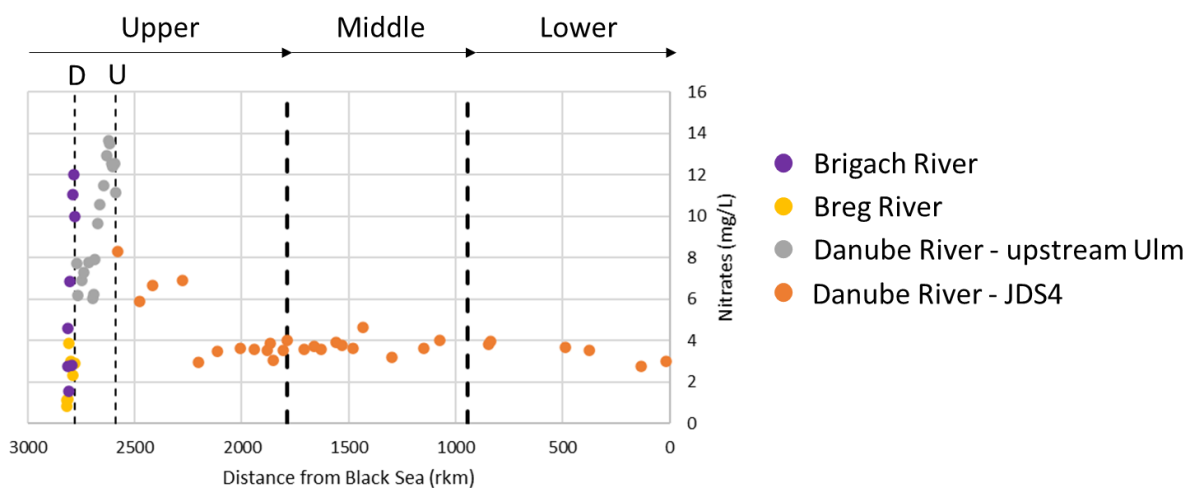


Figure 6: Nitrates along the Danube River. D = Donaueschingen, U = Ulm.

In conclusion, once the Danube River meets its first large tributaries (Iller River in Ulm and Inn River in Passau) the potential anthropogenic pressure exerted by the watershed is rather diffuse and no hot spot can be detected, either for nitrogen species or dissolved organic carbon. In particular, the dissolved organic carbon is slowly increasing, which can be explained by the increase of the served population from upstream to downstream.

3.2. REE spectra and anomalies

Figure 7 shows the REE normalized patterns for the Breg River and the Brigach River. The most upstream section of both rivers present patterns with flat sections between Dy and Lu (Heavy REE or HREE). These patterns are similar to those observed by Louis et al. (2020) for headwaters in the Vosges mountains, running on a similar geology (granite, sandstone). A negative Ce anomaly, induced by the redox characteristics of cerium, can be noticed for both rivers (Elderfield et al., 1990). Indeed, Ce can have two oxidation states (Ce^{3+} and Ce^{4+}) in the typical conditions of temperature and pressure of surface water and Ce^{4+} is likely to combine with oxygen to form cerianite. As cerianite is very insoluble, its formation leads to Ce negative anomaly in water (Seto and Akagi, 2008). Along the Danube River, all samples but two exhibit a negative Ce anomaly (Figure S5) with an average value (\pm one standard deviation) of 0.66 ± 0.14 between Donaueschingen and Ulm and a slight trend downstream of Ulm (coefficient of determination $R^2 = 0.14$).

The La/Lu ratio varies between 0.05 and 0.35 in the Breg and Brigach river and tends to increase along their courses indicating a gradual depletion in LREE with respect to HREE (Figure S6). No clear trend is observed between Donaueschingen and Ulm for the La/Lu ratio because of the variable geology (marlstone, limestone) of the Danube basin in this section combined with possible anthropogenic influences (see below). The sampling is not sufficiently dense in this section to go deeper in the discussion. Between Passau (junction with the Inn River) and the Black Sea, the La/Lu ratio decreases slowly ($R^2 = 0.18$), revealing an increasing fractionation of the REE pattern. The observed decrease indicates increasing inputs from urban and industrial wastewater treatment plants along the Danube River, in agreement with the

increase in sodium concentration. Indeed, highly fractionated REE patterns with LREE depletion and marked Gd anomalies are typical of wastewaters (Martin et al., 2021). The explored tributaries present La/Lu ratios lower than those observed on the Danube River, suggesting a more marked impact of wastewater discharges in these water courses.

Gd anomalies are detected on the Breg River at the Vörenbach station (Be4) and on the Brigach River at the Sankt Georgen station (Bi3), about 10 km downstream their sources. All the samples collected between Donaueschingen and Ulm present a strong Gd anomaly (between 2.8 at station D2 and 10.9 at station D12).

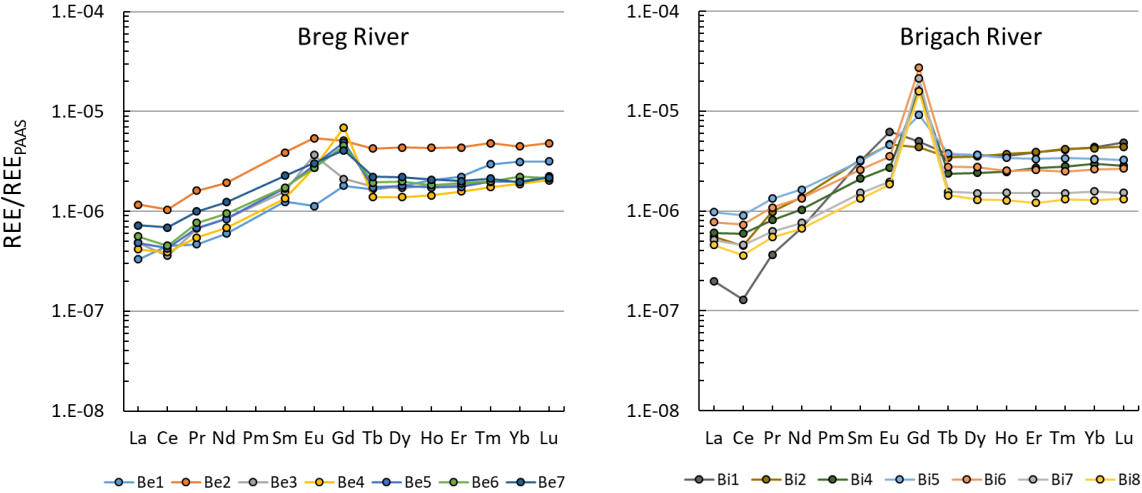


Figure 7: REE patterns, normalized with respect to PAAS, along the Breg River and the Brigach River

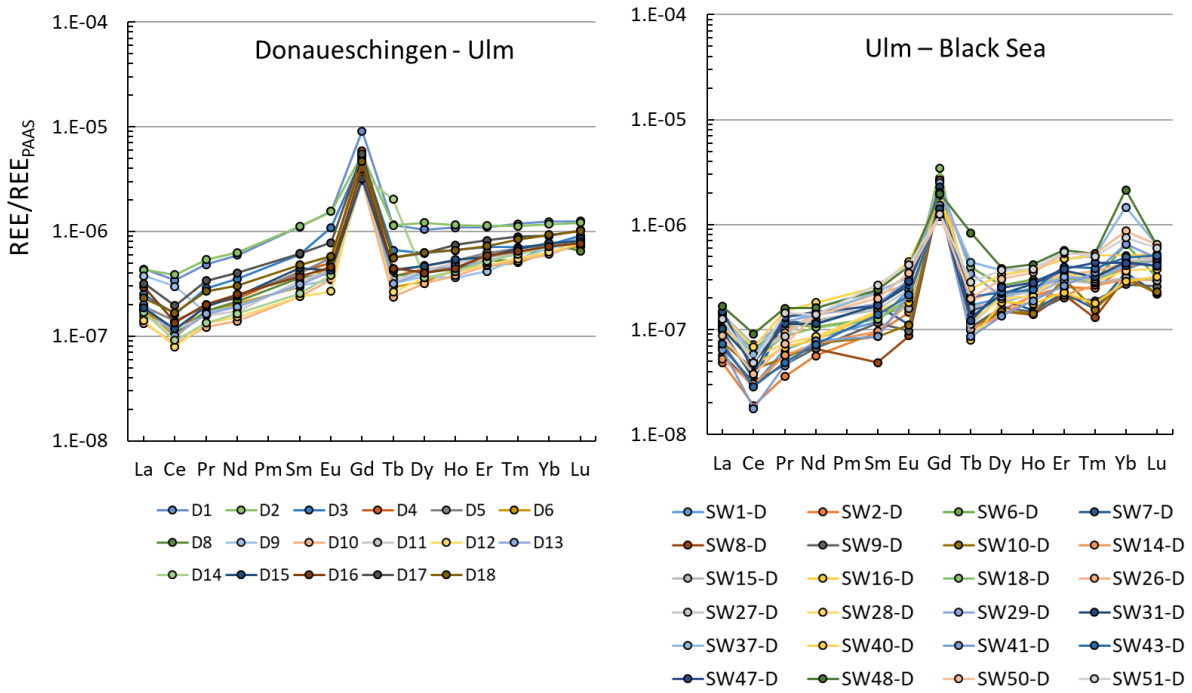


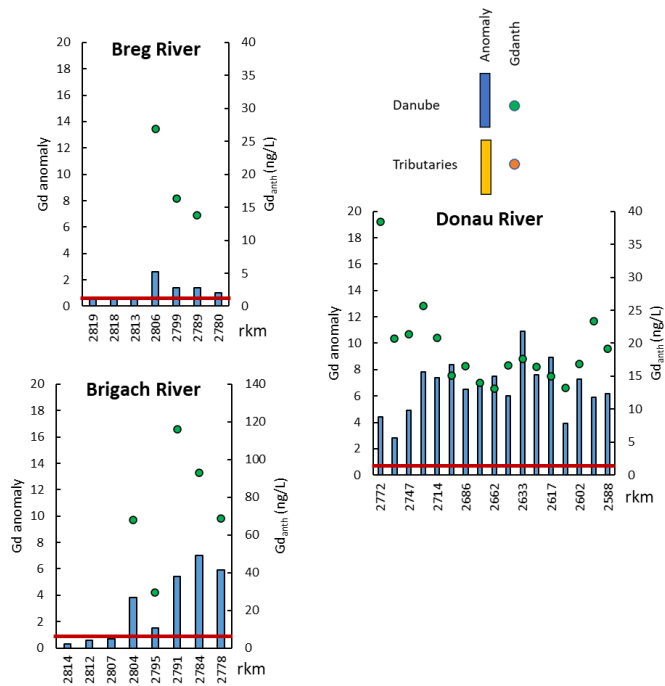
Figure 8: REE patterns, normalized with respect to PAAS, along the Danube River, downstream Donaueschingen

Further downstream, the Gd positive anomaly is detectable in all the samples (Gd/Gd^* value from 1.85 to 37.41), except in sample SW-46 (Russenski Lom, tributary in Bulgaria with $Gd/Gd^*=1.18$) (Figures 8 and S4). To define a Gd anomaly as an anthropogenic anomaly, the threshold value of Gd/Gd^* is usually set to 1.5 (Bau et al., 2006). In the case of the Danube River and its tributaries, the visible Gd anomalies are always above this threshold value: that allows the calculation of Gd_{anth} concentrations. For the Danube River itself, the most important Gd/Gd^* value is for the sample JDS4-4 (Gd/Gd^* : 25.9). This sampling station is located in Germany, just downstream a WWTP effluent discharge.

Only one other study has reported a positive Gd anomaly in Danube River. This is by Kulaksız and Bau (2011b), who analysed a sample grabbed in Austria. Using their data with the Nd and Dy calculation method, the Gd/Gd* anomaly is 2.8 and the Gd_{anth} concentration is estimated at 47 ng/L. The JDS4 samples from SW6-D to SW10-D were collected in Austria. Their Gd/Gd* values are higher (from 10.8 to 18.1) for a lower calculated Gd_{anth} concentration (from 8.3 to 9.5 ng Gd_{anth}/L), which can be explained by the fact that the overall REE amounts for JDS4 are lower than for the study by Kulaksız and Bau, (2011b). However, as the exact location and sampling period of the Kulaksız and Bau (2011b) study are not known and it is difficult to establish a meaningful comparison.

Based on the values of Gd/Gd* and the corresponding calculated Gd_{anth} concentrations two groups can be identified clearly along the Danube River and in its tributaries: from sample SW-D1 (Boefinger Halede) to sample SW-D31 (Ilok), with a Gd/Gd* globally above 10 and from sample SW-32 (Tisza) to sample SW-51D (Vilkova), with a Gd/Gd* globally below 10. Gd anomaly and Gd_{anth} concentration in these two groups can be related to the number of MRI units and MRI exams in each crossed country (Fig. 10). It is interesting to note that the average Gd_{anth} concentration between SW1 and SW31 (11 ng/L \pm 2.5 n/L) is quite stable and does not closely follow the fluctuations in Gd anomalies.

a)



b)

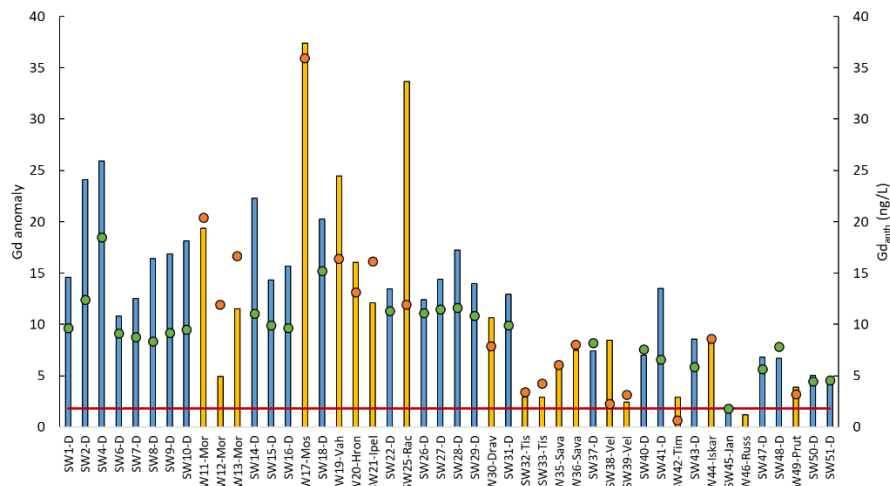


Figure 9: Gd anomaly and Gd_{anth} concentration downstream from the sources to Ulm (a) and from Ulm to the delta (b) for the Danube River and its tributaries. The red line corresponds to the limit value of Gd/Gd^* (1.5) proposed by Bau et al. (2006).

Figure 10 was built using data on the location and capacity of wastewater treatment plants along the Danube River and its main tributaries (expressed in persons-equivalent served). The data were collected from the Urban Waste Water Treatment Directive dissemination platform for EU countries (2016 data) and ICPDR data for non-EU countries. A total of 1546 wastewater treatment plants was considered. For each tributary, the contribution in terms of population to the Danube River watershed was also taken into account, as well as the eventual sharing of the tributary watershed between different countries.

In the first group (Austria, Czech Republic, Slovakia, Hungary, Croatia), the number of MRI exams/year/inhabitants is between 4,000 and 6,000, while it exceeds 14,000 exams/year/inhabitants in Germany (Figure S7). In the second group (Serbia, Bulgaria, Romania), MRI exams/year/inhabitants are below 2,000 and data are missing for Moldavia and Ukraine. The low number of MRI exams in Bulgaria can explain why there is no Gd/Gd* detected in sample JDS4-46. The tipping point, where Gd/Gd* becomes lower than 10, is Ilok (Croatia) (i.e. SW31-D). We note that the sampling plan of JDS4 for the Danube Delta region included only one site in the Chilia arm. The possible impact of the large city of Tulcea on REE pattern in the Sulina and Sfantu Gheorghe arms of the Danube Delta would require further consideration.

The groundwater wells close to the Danube River are also affected by anthropogenic Gd (Fig. S8). Gd-containing contrasting agents are synthesized not to easily release ionic Gd^{3+} , which is extremely toxic, inside the human body. This otherwise desirable property makes them particularly difficult to degrade during drinking water treatment production and explains the presence of Gd in tap water.

It can be expected that the situation will not improve in the near future (Lachaux et al., 2022). The risk associated with Gd might even increase with the application of advanced technologies designed to degrade urban micropollutants in wastewater treatments plants, with the ultimate goals to reduce aquatic ecosystems contamination on one hand and potentially reuse treated wastewater on another hand. The risk associated with the dissemination of free Gd³⁺ cannot be ignored considering the possible degradation of Gd-based contrast agents (Oluwasala et al., 2022).

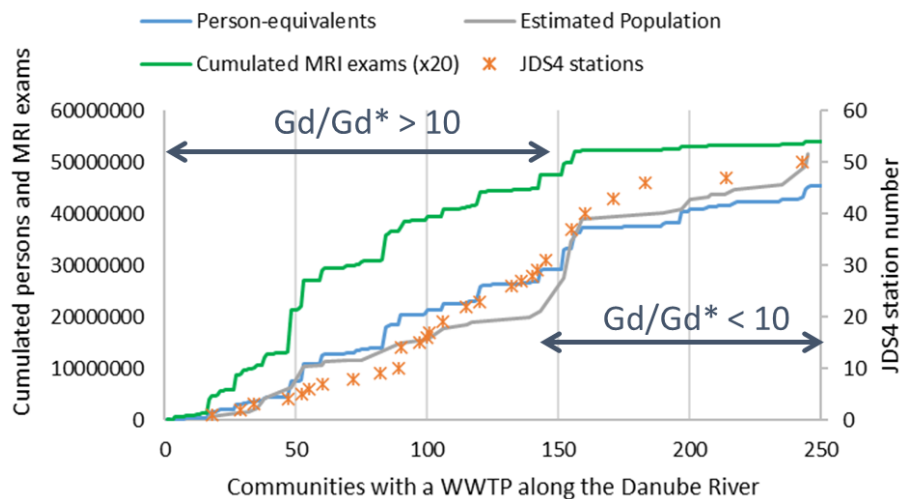


Figure 10: Gd anomaly in the Danube River watershed in as a function of the population and the number of MRI exams

The annual flux of Gd_{anth} to the Black Sea, based on a total discharge just upstream of the delta of 6,500 m³/sec, is estimated at 0.9 ton/year, corresponding to 11 kg/year/million inhabitants. This is of the same order of magnitude as the flux discharged by the Garonne River in France (14 kg/year/million inhabitants) (Lerat-Hardy et al., 2019). The annual flux is comparable with the annual flux of other large watersheds, such as the Saint-Laurent Estuary and Gulf in Canada

(0.9 ± 0.7 ton/year) (Dang et al., 2022) and the Pearl River (0.6 ± 0.6 ton/year for about 84 million inhabitants) (Ma and Wang, 2023).

Finally, an Ytterbium anomaly seems to appear at some sampling sites close to the delta, in particular in stations SW-D37 and SW-D48. This anomaly is also clear on two tributaries, the Sava River and the Velika Morava River. No information related to such an anomaly could be found in the literature. Ytterbium is not largely used: its main uses are related to the improvement of stainless-steel properties and the production of lasers. However, sedimentary phosphate deposits (Emsbo et al., 2015) and their dumped residues from fertilizer production can contain ytterbium (Zirnea et al., 2013), which can be leached toward water bodies.

4. Conclusions

At short distance from their sources the Brigach River and Breg River present REE patterns already influenced by the release in the aquatic environment of anthropogenic Gd. The Gd concentration in the Danube River is influenced by the development of MRI facilities and examinations. The slow decrease of the La/Lu ratio between Ulm and the Black Sea indicates an increasing anthropogenic influence as the Danube River flows downstream. As this survey was the first one to analyze REEs in the Danube River basin, future work will focus on consolidating the data with an increase of the number of sampling points in the Middle and Lower sections of the Danube as well as along the largest tributaries. Analysis of sediments could also bring information on the distribution of REE in the watershed. Although the monitoring of REE and the understanding of their origin and fate in large and complex

watersheds are not easy tasks, they should be pursued, taking the example of the logistics developed during JDS4.

Acknowledgments

The authors acknowledge the financial support from the National Agency for Research – France (ANR) through the project ANR-16-CE34-0012-001 and of the LIFE Program (ENV.780956). The support of ICPDR and Norman network is greatly acknowledged.

References

- Alkan, A., Alkan, N., Yanar, B. 2020. Investigation of pollution levels originated from anthropogenic gadolinium in Ankara Stream. *Environ. Sci. Pollut. R.*, 27, 23677–23685. <https://doi.org/10.1007/s11356-020-08702-7>.
- Amyot, M., Clayden, M.G., MacMillan, G.A., Perron, T., Arscott-Gauvin, A. 2017. Fate and trophic transfer of rare earth elements in temperate lake food webs. *Environ. Sci. Technol.*, 51, 6009-6017. <https://doi.org/10.1021/acs.est.7b00739>
- Andrade, R.L.B., Hatje, V., Pedreira R.M.A., Böning, P., Pahnke, K., 2020. REE fractionation and human Gd footprint along the continuum between Paraguaçu River to coastal South Atlantic waters. *Chem. Geol.*, 532, 119303. <https://doi.org/10.1016/j.chemgeo.2019.119303>

- Assaad, A., Pontvianne, S., Corriou, J.P., Pons, M.N. (2015) Spectrophotometric characterization of dissolved organic matter in a rural watershed: the Madon River (N-E France), *EMAS*, 187, 188, <https://doi.org/10.1007/s10661-015-4422-9>
- Baker, A., 2002. Fluorescence properties of some farm wastes: implications for water quality monitoring. *Wat. Res.*, 36, 189-195, [https://doi.org/10.1016/s0043-1354\(01\)00210-x](https://doi.org/10.1016/s0043-1354(01)00210-x).
- Bau, M., Dulski, P., 1996. Anthropogenic origin of positive gadolinium anomalies in rivers waters. *Earth Planet. Sc. Lett.*, 143, 245-255. [https://doi.org/10.1016/0012-821X\(96\)00127-6](https://doi.org/10.1016/0012-821X(96)00127-6)
- Bau, M., Knappe, A., Dulski, P., 2006. Anthropogenic gadolinium as a micropollutant in river waters in Pennsylvania and in Lake Erie, northeastern United States. *Chem. Erde*, 66, 143-152. <https://doi.org/10.1016/j.chemer.2006.01.002>
- Becci, A., Boelchini, F., Amato, A., 2021. Sustainable strategies for the exploitation of end-of-life permanent magnets. *Processes*, 9, 857. <https://doi.org/10.3390/pr9050857>
- Boester, U., Rude, T.R., 2020. Utilize gadolinium as environmental tracer for surface water-groundwater interaction in Karst. *J. Contam. Hydrol.*, 235, 103710. <https://doi.org/10.1016/j.jconhyd.2020.103710>
- Chazot, A., Barrat, J.A., Jomaah, R., Ognard, J., Ben Salem, D. 2020. Gaha, M., Brain MRIs makeup the bulk of the gadolinium footprint in medical imaging. *J. Neuroradiology* 47, 259–265. <https://doi.org/10.1016/j.neurad.2020.03.004>
- Chen, Y., Huang, R., Guan, Y., Zhuang, T., Wang, Y., Tan, T., Wang, J., Zhou, R., Wang, B., Xu, J., Zhang, X., Zhou, K., Sun, R., Chen, M., 2021. The profiling of elements and pesticides in

surface water in Nanjing, China with global comparisons. *Sci. Tot. Envir.*, 774, 145749.

<https://doi.org/10.1016/j.scitotenv.2021.145749>.

Coble, P.G., 1996. Characterization of marine and terrestrial DOM in seawater using excitation-emission spectroscopy. *Mar. Chem.*, 51, 325-346,

[https://doi.org/10.1016/0304-4203\(95\)00062-3](https://doi.org/10.1016/0304-4203(95)00062-3).

Dale, J.G., Cox, S.S., Vance, M.E., Marr, L.C., Hochella Jr, M.F., 2017. Transformation of cerium oxide nanoparticles from a diesel fuel additive during combustion in a diesel engine.

Environ. Sci. Technol., 51, 1973–1980. <https://doi.org/10.1021/acs.est.6b03173>

Dang, D.H., Wang, W., Silma, A., Chatzis, A., Mucci, A., 2022. The contrasting estuarine geochemistry of rare earth elements between ice-covered and ice-free conditions.

Geochim. Cosmochim. Acta 317, 488–506. <https://doi.org/10.1016/j.gca.2021.10.025>

Elderfield, H., Upstill-Goddard, R., Sholkovitz, E.R., 1990. The rare earth elements in rivers, estuaries, and coastal seas and their significance to the composition of ocean waters.

Geochim. Cosmochim. Acta 54, 971–991. [https://doi.org/10.1016/0016-7037\(90\)90432-K](https://doi.org/10.1016/0016-7037(90)90432-K)

Emsbo, P., McLaughlin, P.I., Breit, G.N., du Bray E.A., Koenig, A.E. 2015. Rare earth elements in sedimentary phosphate deposits: Solution to the global REE crisis? *Gondwana Res.* 27,

776–785. <http://dx.doi.org/10.1016/j.gr.2014.10.008>

Fraum, T.J., Ludwig, D.R., Bashir, M.R., Fowler, K.J., 2017. Gadolinium-based contrast agents: a comprehensive risk assessment. *J. Magn. Reson. Imaging.* 46(2), 338-353. <https://doi.org/10.1002/jmri.25625>

- Han, R., Wang, Z., Shen, Y., Wu, Q., Liu, X., Cao, C., Gao, S., Zhang, J., 2021. Anthropogenic Gd in urban river water: A case study in Guiyang, SW China. *Elem. Sci. Anth.*, 9: 1. DOI: <https://doi.org/10.1525/elementa.2020.00147>
- Hissler, C., Hostache, R., Iffly, J.F., Pfister, L., Stille, P., 2015. Anthropogenic rare earth element fluxes into floodplains: Coupling between geochemical monitoring and hydrodynamic sediment transport modelling. *Comptes Rendus Geosci.* 347, 294–303. <http://dx.doi.org/10.1016/j.crte.2015.01.003>
- Hobohm, J., Kuchta, K., Krüger, O., van Wasen, S., Adam, C., 2016. Optimized elemental analysis of fluorescence lamp shredder waste. *Talanta* 147, 615-620. <http://dx.doi.org/10.1016/j.talanta.2015.09.068>
- Hu, Z., Richet, H., Sparovek, G., Schnug, E., 2004. Physiological and biochemical effects of rare earth elements on plants and their agricultural significance: a review. *J. Plant Nutr.*, 271, 183-220. <https://doi.org/10.1081/PLN-120027555>
- Inoue, K., Fukushi, M., Furukawa, A., Sahoob, S.K., Veerasamy, N., Ichimura, K., Kasahara, S., Ichihara, M., Tsukada, M., Torii, M., Mizaghuchi, M., Taguchi, Y., Nakazawa, S. 2020. Impact on gadolinium anomaly in river waters in Tokyo related to the increased number of MRI devices in use. *Mar. Pollut. Bull.* 154, 111148. <https://doi.org/10.1016/j.marpolbul.2020.111148>
- Joint Danube Survey 3. A Comprehensive Analysis of Danube Water Quality. 2015. Eds: Liška, I., Wagner, F., Sengl, M., Deutsch, K. Slobodník, J. ISBN: 978-3-200-03795-3, Vienna, Austria. (http://www.danubesurvey.org/jds3/jds3-files/nodes/documents/jds3_final_scientific_report_1.pdf)

- JDS4 Scientific Report: A Shared Analysis of the Danube River Basin. 2021. Eds: Liška, I., Wagner, F., Sengl, M., Deutsch, K. Slobodník, J., Paunović, M. ISBN: 978-3-200-07450-7, Vienna, Austria. (<http://www.danubesurvey.org/jds4/publications/scientific-report>)
- Kaegi, R., Gogos, A., Voegelin, A., Hug, S.J., Winkel, L.H.E., Buser, A.M., Berg, M., 2021. Quantification of individual Rare Earth Elements from industrial sources in sewage sludge. *Water Res. X*, 11, 1000092. <https://doi.org/10.1016/j.wroa.2021.100092>
- Khan, A.M., Yusoff, I., Abu Bakar, N.K., Abu Bakar, A.F., Alias, Y., 2016. Assessing anthropogenic levels, speciation, and potential mobility of rare earth elements (REEs) in ex-tin mining area. *Environ Sci. Pollut. Res.*, 23, 25039–25055. <https://doi.org/10.1007/s11356-016-7641-x>
- Kim, I., Kim, S.H., Kim, G., 2020. Anthropogenic gadolinium in lakes and rivers near metrocities in Korea. *Environ. Sci.: Processes Impacts*, 22, 144. <https://doi.org/10.1039/c9em00304e>
- Kondor, A.C., Jakab, G., Vancsik, A., Filep, T., Szeberényi, J., Szabó L., Maász, G., Ferincz, A., Dobosy, P., Szalai, Z., 2020. Occurrence of pharmaceuticals in the Danube and drinking water wells: Efficiency of riverbank filtration. *Environ. Pollut.*, 265, 114893. <https://doi.org/10.1016/j.envpol.2020.114893>
- Kulaksız, S., Bau, M., 2011a. Rare earth elements in the Rhine River, Germany: First case of anthropogenic lanthanum as a dissolved microcontaminant in the hydrosphere. *Environ. Int.* 37, 973-979. <https://doi.org/10.1016/j.envint.2011.02.018>
- Kulaksız, S., Bau, M., 2011b. Anthropogenic gadolinium as a microcontaminant in tap water used as drinking water in urban areas and megacities. *Appl. Geochem.*, 26, 1877-1885. <https://doi.org/10.1016/j.apgeochem.2011.06.011>

- Kulaksız, S., Bau, M., 2013. Anthropogenic dissolved and colloid/nanoparticle-bound samarium, lanthanum and gadolinium in the Rhine River and the impending destruction of the natural rare earth element distribution in rivers. *Earth Planet Sc. Lett.*, 362, 43-50. <https://doi.org/10.1016/j.epsl.2012.11.033>
- Lachaux, N., Cossu-Leguille, C., Poirier, L., Gross, E.M., Giamberini, L., 2022. Integrated environmental risk assessment of rare earth elements mixture on aquatic ecosystems. *Front. Environ. Sci.* 10:974191. <https://doi.org/10.3389/fenvs.2022.974191>.
- Lavezzo, B., Kinoshita, A., Figueiredo, A.M.G., Pinheiro, M.M.F., Santa, W. 2020. Detection of rare-earth elements using fiddler crabs *Leptuca leptodactyla* (Crustacea: Ocypodidae) as bioindicators in mangroves on the coast of São Paulo, Brazil. *Sci. Tot. Envir.*, 738, 139787. <https://doi.org/10.1016/j.scitotenv.2020.139787>
- Le Goff, S., Barrat, J.A., Chauvaud, L., Paulet, Y.M., Gueguen, B., Ben Salem, D., 2019. Compound-specific recording of gadolinium pollution in coastal waters by great scallops. *Sci. Rep.*, 9, 8015. <https://doi.org/10.1038/s41598-019-44539-y>
- Lerat-Hardy, A., Coynel, A., Dutruch, L., Pereto, C., Bossy, C., Gil-Diaz, T., Capdeville, M.J., Blanc, G., Schäfer, J. 2019. Rare Earth Element fluxes over 15 years into a major European Estuary (Garonne-Gironde, SW France): Hospital effluents as a source of increasing gadolinium anomalies. *Sci. Tot. Envir.*, 656, 400-420. <https://doi.org/10.1016/j.scitotenv.2018.11.343>
- Liu, W.S., Guo, M.N., Liu, C., Yuan, M., Chen, X.T., Huot, H., Zhao, C.M., Tang, Y.T., Morel, J.L., Qiu, R.L., 2019. Water, sediment and agricultural soil contamination from an ion adsorption rare earth mining area. *Chemosphere*, 216, 75-83. <https://doi.org/10.1016/j.chemosphere.2018.10.109>

- Lortholarie, M., Zalouk-Vergnoux, A., Couderc, M., Kamari, A., François, Y., Herrenknecht, C., Poirier, L., 2020. Rare earth element bioaccumulation in the yellow and silver European eel (*Anguilla anguilla*): A case study in the Loire estuary (France). *Sci. Tot. Envir.*, 719, 134938.
<https://doi.org/10.1016/j.scitotenv.2019.134938>
- Louis, P., Messaoudene, A., Jrad, H., Adboul-Hamid, B.A., Vignati, D.A.L., Pons, M.N., 2020. Understanding Rare Earth Elements concentrations, anomalies and fluxes at the river basin scale: the Moselle River (France) as a case study. *Sci. Tot. Envir.*, 742, 140619.
<https://doi.org/10.1016/j.scitotenv.2020.140619>
- Ma, L., Wang, W.X. 2023. Dissolved rare earth elements in the Pearl River Delta: Using Gd as a tracer of anthropogenic activity from river towards the sea. *Sci. Tot. Envir.*, 856, 159241,
<http://dx.doi.org/10.1016/j.scitotenv.2022.159241>.
- Martin, L.A., Vignati, D.A.L., Hissler, C. 2021. Contrasting distribution of REE and yttrium among particulate, colloidal and dissolved fractions during low and high flows in peri-urban and agricultural river systems. *Sci. Tot. Envir.*, 790, 148207,
<http://dx.doi.org/10.1016/j.scitotenv.2021.148207>
- McLennan, S.M., 1989. Rare earth elements in sedimentary rocks; influence of provenance and sedimentary processes. *Rev. Mineral. Geochem.* 21, 169–200.
- Merschel, G., Bau, M., 2015. Rare earth elements in the aragonitic shell of freshwater mussel *Corbicula fluminea* and the bioavailability of anthropogenic lanthanum, samarium and gadolinium in river water. *Sci. Tot. Envir.*, 533, 91-101,
<http://dx.doi.org/10.1016/j.scitotenv.2015.06.042>

- Möller, P., Paces, T., Dulski, P., Morteani, G., 2002. Anthropogenic Gd in surface water, drainage system, and the water supply of the city of Prague, Czech Republic. *Environ. Sci. Technol.* 36, 2387-2394. <https://doi.org/10.1021/es010235q>
- Möller, P., Morteani, G., Dulski, P. 2003. Anomalous gadolinium, cerium, and yttrium contents in the Adige and Isarco river waters and in the water of their tributaries (provinces Trento and Bolzano/Bozen, NE Italy). *Acta Hydrochim. Hydrobiol.* 31, 3, 225–239. <https://doi.org/10.1002/aheh.200300492>
- Mouchi, V., Godbillot, C., Forest, V., Ulianov, A., Lartaud, F., de Rafélis, M., Emmanuel, L., Verrecchia, E.P., 2020. Rare earth elements in oyster shells: provenance discrimination and potential vital effects. *Biogeosciences*, 17, 2205–2217. <https://doi.org/10.5194/bg-17-2205-2020>
- Nozaki, Y., Lerche, D., Alibo, D.S., Tsutsumi, M., 2000. Dissolved indium and rare earth elements in three Japanese rivers and Tokyo Bay: Evidence for anthropogenic Gd and In. *Geochim. Cosmochim. Acta* 64, 3975–3982.
- Ogata, T., Terakado, Y., 2006. Rare earth element abundances in some seawaters and related river waters from the Osaka Bay area, Japan: Significance of anthropogenic Gd. *Geochem. J.*, 40, 463-474. <https://doi.org/10.2343/geochemj.40.463>
- Oluwasola, I.E., Ahmad, A.L., Shoparwe, N.F., Ismail S., 2022. Gadolinium based contrast agents (GBCAs): Uniqueness, aquatic toxicity concerns, and prospective remediation. *J. Contam. Hydrol.* 250, 104057. <https://doi.org/10.1016/j.jconhyd.2022.104057>.

- Pereto, C., Coynel, A., Lerat-Hardy, A., Gourves, P.Y., Schäfer, J., Baudrimont, M., 2020. *Corbicula fluminea*: A sentinel species for urban Rare Earth Element origin. *Sci. Tot. Envir.*, 732, 138552. <https://doi.org/10.1016/j.scitotenv.2020.138552>
- Porvali, A., Agarwal, V., Lundström, M., 2020. REE(III) recovery from spent NiMH batteries as REE double sulfates and their simultaneous hydrolysis and wet-oxidation. *Waste Manage.* 107, 66-73. <https://doi.org/10.1016/j.wasman.2020.03.042>
- Rabiet, M., Brissaud, F., Seidel, J.L., Pistre, S., Elbaz-Poulichet, F., 2009. Positive gadolinium anomalies in wastewater treatment plant effluents and aquatic environment in the Hérault watershed (South France). *Chemosphere* 75, 1057–1064. <https://doi.org/10.1016/j.chemosphere.2009.01.036>
- Rétif, J., Zalouk-Vergnoux, A., Briant, N., Poirier, L. 2023. From geochemistry to ecotoxicology of rare earth elements in aquatic environments: Diversity and uses of normalization reference materials and anomaly calculation methods. *Sci. Tot. Envir.*, 856, 158890. <http://dx.doi.org/10.1016/j.scitotenv.2022.158890>.
- Santos, A.C.S.S., Souza, L.A., Araujo, T.G., de Rezende, C.E., Hatje, V. 2023. Fate and trophic transfer of rare earth elements in a tropical estuarine food web. *Environ. Sci. Technol.*, 57, 2004-2014. <https://doi.org/10.1021/acs.est.2c07726>.
- Seto, M., Akagi T. (2008) Chemical condition for the appearance of a negative Ce anomaly in stream waters and groundwaters. *Geochem. J.*, 42: 371-380. <https://doi.org/10.2343/geochemj.42.371>
- Shajib, M.T.I., Hansen, H.C.B., Liang, T., Holm, P.E., 2020. Rare earth elements in surface specific urban runoff in Northern Beijing. *Sci. Tot. Envir.*, 717, 136969. <https://doi.org/10.1016/j.scitotenv.2020.136969>

- Song, H., Shin, W.J., Ryu, J.S., Shin, H.S., Chung, H., Lee, K.S., 2017. Anthropogenic rare earth elements and their spatial distributions in the Han River, South Korea. *Chemosphere*, 172, 155-165. <https://doi.org/10.1016/j.chemosphere.2016.12.135>
- Souza, L.A., Pedreira, R.M.A., Miró, M., Hatje, V., 2021. Evidence of high bioaccessibility of gadolinium-contrast agents in natural waters after human oral uptake. *Sci. Tot. Envir.*, 793, 148506. <https://doi.org/10.1016/j.scitotenv.2021.148506>
- Tepe, N., Romeo, M., Bau, M., 2014. High-technology metals as emerging contaminants: Strong increase of anthropogenic gadolinium levels in tap water of Berlin, Germany, from 2009 to 2012. *Appl. Geochem.*, 45, 191-197. <http://dx.doi.org/10.1016/j.apgeochem.2014.04.006>
- Thomsen, H.S. 2017. Are the increasing amounts of gadolinium in surface and tap water dangerous? *Acta Radiol.*, 8(3) 259–263. <https://doi.org/10.1177/0284185116666419>
- Turra, C., 2018. Sustainability of rare earth elements chain: from production to food – a review. *Int. J. Environ. Heal. R.*, 2, 1, 23-42. <https://doi.org/10.1080/09603123.2017.1415307>
- Valdés-Vilchis, S., Sánchez-Beristain, J.P., Bernal, C., Juárez, E.A., 2021. Rare Earth Elements and Yttrium (REE+Y) patterns in recent *Anadara brasiliiana* shells from Playa Norte, Barra de Cazonos (Veracruz, Mexico): Evidence of anthropogenic contamination linked to river output? *J. S. Am. Earth Sci.*, 110, 103368. <https://doi.org/10.1016/j.jsames.2021.103368>
- Veiga, M., Mattiazzi, P., de Gois, J.S., Nascimento, P.C., Borges, D.L.G., Bohrer, D., 2020. Presence of other rare earth metals in gadolinium-based contrast agents. *Talanta* 216, 120940. <https://doi.org/10.1016/j.talanta.2020.120940>

- Yang, Y., Walton, A., Sheridan, R., Güth, K., Gauß, R., Gutfleisch, O., Buchert, M., Steenari, B.-M., Van Gerven, T., Jones, P.T., Binnemans, K., 2017. REE recovery from end-of-life NdFeB permanent magnet scrap: a critical review. *J. Sustain. Metall.*, 3, 122–149. <https://doi.org/10.1007/s40831-016-0090-4>
- Yeghicheyan, D., Aubert, D., Bouhnik-Le Coz, M., Chmeleff, J., Delpoux, S., Djouaraev, I., Granier, G., Lacan, F., Piro, J., Rousseau, T., Cloquet, C., Marquet, A., Menniti, C., Pradoux, C., Freydier, R., Vieira da Silva-Filho, E., Suchorski, K., 2019. A new interlaboratory characterisation of silicon, rare earth elements and twenty-two other trace element concentrations in the natural river water certified reference material SLRS -6 (NRC - CNRC). *Geostand. Geoanalytical Res.* 43, 475–496. <https://doi.org/10.1111/ggr.12268>
- Zabrecky, J.M., Liu, X.-M., Wu, Q., Cao, C. 2021. Evidence of anthropogenic Gadolinium in Triangle Area Waters, North Carolina, USA. *Water*, 13, 1895. <https://doi.org/10.3390/w13141895>
- Zhang, C., Wang, L., Zhang, S. 1998. Geochemistry of rare earth elements in the mainstream of the Yangtze River, China. *Appl. Geochem.*, 13, 451-462. [https://doi.org/10.1016/S0883-2927\(97\)00079-6](https://doi.org/10.1016/S0883-2927(97)00079-6)
- Zirnea, S., Lazar, I., Saha Foudjoa B.U., Vasilache, T., Lazar, G., 2013. Cluster analysis based of geochemical properties of phosphogypsum dump located near Bacau City in Romania. *APCBEE Procedia* 5, 317 – 322. <https://doi.org/10.1016/j.apcbee.2013.05.05>.

Spatial distribution of Rare Earth Elements in a transnational watershed: the case of the Danube River

Pauline LOUIS¹, Davide A.L. VIGNATI², Steve PONTVIANNE¹, Marie-Noëlle PONS^{1,3*}

1 Université de Lorraine, CNRS, LRGP, F-54000 Nancy, France

2 Université de Lorraine, CNRS, LIEC, F-57000 Metz, France

3 LTSEZ-Zone Atelier du Bassin de la Moselle, LRGP, 54000, Nancy, France

Supplementary Information

Table S1: Non-exhaustive list of rivers sampled for Gd content around the world

Stream and country	Gd average or range (ng/L)	Nb of sampling points	Comments	Reference
Västerdalälven River, Sweden	41.6	1	Station: Lima Dalama	Bau and Dulski, 1996
Elbe, Germany	5.7	1	Station: Nienstetten	Bau and Dulski, 1996
Mosel River, Germany	4.6	1	Wasserbilligerbrück,	Bau and Dulski, 1996
Spree River, Germany	6.7	1	Berlin	Bau and Dulski, 1996
Spree River, Germany	1.7 - 15	2	Berlin urban area	Knappe et al, 2005
Havel River, Germany	106	1	Postdam	Bau and Dulski, 1996
Havel River, Germany	3 – 123	7	Berlin urban area	Knappe et al, 2005
Havel River, Germany	492	1		Kulakzic and Bau, 2011b
Wupper River, Germany	32.5	1	Leverkusen	Bau and Dulski, 1996

Dahme River, Germany	1.2	1	Berlin	Knappe et al, 2005
Rhine River, Germany	8.6	1	Düsseldorf	Bau and Dulski, 1996
Rhine, Germany & Netherlands	5.3 – 34.9	3	Leverkusen - Leerdam	Kulakzic and Bau, 2013
Rhine River, Germany	11.9 – 126	10	Reach length: 500 km	Kulakzic & Bau 2011a
Danube River, Austria	7.6	1		Kulakzic and Bau, 2011b
Thames River, UK	4.4	1		Kulakzic and Bau, 2011b
Mosel River, France	2 - 111	39 63 (tributaries)	Reach length: 314 km	Louis et al., 2020
Vene River, France	1.3 – 3	1		Elbaz-Poulichet et al., 2002
Garonne River, France	3.61 – 20	1	Time range: 2003 - 2017	Lerat-Hardy et al., 2019
Adige River, Italy	0.5	3		Möller et al., 2003
Dommel River and tributaries, Netherlands	20 - 173	7	Several campaigns	Petelet-Giraud et al., 2009
Vltava River and tributaries, Czech Republic	0.9 – 44.7	22	Range of Gd _{ant}	Morteani et al., 2006
Ankara Stream and its tributaries, Turkey	15 ± 5 / 347 ± 57	7	Reach length: 90 km	Alkan et al., 2020
Pensylvania rivers, USA	3.75 – 31.9	12		Bau et al. 2006
Three rivers in Neuse River Basin USA	26.4 - 390	9		Zabrecky et al., 2021

Paraguaçu River, Brazil	4.2	1		Andrade et al., 2020
Atibaia River & Anhumas Creek, Brazil	5.9 – 56	22		Campos and Enzweiler, 2016
St Lawrence River, Canada	3.1 – 132	18		Dang et al., 2022
Toshibetsu River, Japan	12.2	1	Station: Aikkapu	Bau and Dulski, 1996
Rivers (10) of Tokyo Metropolitan Area, Japan	0.3 – 140	40	Distance between the most upstream station and the sea: 60 km	Inoue et al., 2020
Tama River, Ara River, Tone River, Japan	3.9 - 24 4.1 – 10.4 1.6 – 9.2	3 4 4		Nozaki et al., 2000
Yodo River, Muko River, Japan	3.93 21.7	2 2		Ogata et al., 2006
Han River and 7 tributaries, South Korea	2.7– 90	6 2	Reach length: 50 km	Song et al., 2017
Youyu River, Baiyan River, Jinzhong River, China	0.43 to 86.65	9 6 3		Zhang et al., 2019
Nanming River, China	1.38 – 35.42	13	Reach length: 118 km	Han et al, 2021
Pearl River, China	3 – 24.37	15		Ma and Wang, 2023
Cai River, Vietnam	95.8	1		Koukina et al., 2021
Gowrie Creek and tributaries, Australia	0.1 – 145	16	Reach length: 90 km (3 campaigns)	Lawrence and Bariel, 2010

Beerburum Creek, Australia	12.7 – 168.5	12	Reach length: 20 km	Lawrence et al. 2006
22 creeks in Australia	4.3 – 99.3	1 to 2		Lawrence et al.,2006

Alkan, A., Alkan, N., Yanar, B. 2020. Investigation of pollution levels originated from anthropogenic gadolinium in Ankara Stream. *Environ. Sci. Pollut. R.*, 27, 23677–23685. <https://doi.org/10.1007/s11356-020-08702-7>.

Andrade, R.L.B., Hatje, V., Pedreira R.M.A., Böning, P., Pahnke, K., 2020. REE fractionation and human Gd footprint along the continuum between Paraguaçu River to coastal South Atlantic waters. *Chem. Geol.*, 532, 119303. <https://doi.org/10.1016/j.chemgeo.2019.119303>

Bau, M., Dulski, P., 1996. Anthropogenic origin of positive gadolinium anomalies in rivers waters. *Earth Planet. Sc. Lett.*, 143, 245-255. [https://doi.org/10.1016/0012-821X\(96\)00127-6](https://doi.org/10.1016/0012-821X(96)00127-6)

Bau, M., Knappe, A., Dulski, P., 2006. Anthropogenic gadolinium as a micropollutant in river waters in Pennsylvania and in Lake Erie, northeastern United States. *Chem. Erde*, 66, 143-152. <https://doi.org/10.1016/j.chemer.2006.01.002>

Campos, F.F., Enzweiler J., 2016. Anthropogenic gadolinium anomalies and rare earth elements in the water of Atibaia River and Anhumas Creek, Southeast Brazil. *Environ. Monit. Assess.*, 188: 281. <https://doi.org/10.1007/s10661-016-5282-7>

Han, R., Wang, Z., Shen, Y., Wu, Q., Liu, X., Cao, C., Gao, S., Zhang, J., 2021. Anthropogenic Gd in urban river water: A case study in Guiyang, SW China. *Elem. Sci. Anth.*, 9: 1. DOI: <https://doi.org/10.1525/elementa.2020.00147>

Inoue, K., Fukushi, M., Furukawa, A., Sahoob, S.K., Veerasamy, N., Ichimura, K., Kasahara, S., Ichihara, M., Tsukada, M., Torii, M., Mizaguchi, M., Taguchi, Y., Nakazawa, S. 2020. Impact on gadolinium anomaly in river waters in Tokyo related to the increased number of MRI devices in use. *Mar. Pollut. Bull.* 154, 111148. <https://doi.org/10.1016/j.marpolbul.2020.111148>

Kim, I., Kim, S.H., Kim, G., 2020. Anthropogenic gadolinium in lakes and rivers near metrocities in Korea. *Environ. Sci.: Processes Impacts*, 22, 144. <https://doi.org/10.1039/c9em00304e>

Koukina, S.E., Lobus, N.V., Shatravin, A.V. 2021. Multi-element signatures in solid and solution phases in a tropical mixing zone: A case study in the Cai River estuary, Vietnam. *Chemosphere*, 280, 130951. <https://doi.org/10.1016/j.chemosphere.2021.130951>

Kulaksız, S., Bau, M., 2011a. Rare earth elements in the Rhine River, Germany: First case of anthropogenic lanthanum as a dissolved microcontaminant in the hydrosphere. *Environ. Int.* 37, 973-979. <https://doi.org/10.1016/j.envint.2011.02.018>

Kulaksız, S., Bau, M., 2011b. Anthropogenic gadolinium as a microcontaminant in tap water used as drinking water in urban areas and megacities. *Appl. Geochem.*, 26, 1877-1885. <https://doi.org/10.1016/j.apgeochem.2011.06.011>

- Kulaksız, S., Bau, M., 2013. Anthropogenic dissolved and colloid/nanoparticle-bound samarium, lanthanum and gadolinium in the Rhine River and the impending destruction of the natural rare earth element distribution in rivers. *Earth Planet Sc. Lett.*, 362, 43-50. <https://doi.org/10.1016/j.epsl.2012.11.033>
- Lawrence, M.G., Jupiter, S.D., Kamber, B.S., 2006. Aquatic geochemistry of the rare earth elements and yttrium in the Pioneer River catchment, Australia. *Mar. Freshwater Res.* 57, 725–736. <http://doi.org/10.1007/s10498-005-4471-8>
- Lawrence, M.G., Bariel, D.G., 2010. Tracing treated wastewater in an inland catchment using anthropogenic gadolinium. *Chemosphere*, 80: 794-799. <https://doi.org/10.1016/j.chemosphere.2010.05.001>
- Lerat-Hardy, A., Coynel, A., Dutruch, L., Pereto, C., Bossy, C., Gil-Diaz, T., Capdeville, M.J., Blanc, G., Schäfer, J. 2019. Rare Earth Element fluxes over 15 years into a major European Estuary (Garonne-Gironde, SW France): Hospital effluents as a source of increasing gadolinium anomalies. *Sci. Tot. Envir.*, 656, 400-420. <https://doi.org/10.1016/j.scitotenv.2018.11.343>
- Louis, P., Messaoudene, A., Jrad, H., Adboul-Hamid, B.A., Vignati, D.A.L., Pons, M.N., 2020. Understanding Rare Earth Elements concentrations, anomalies and fluxes at the river basin scale: the Moselle River (France) as a case study. *Sci. Tot. Envir.*, 742, 140619. <https://doi.org/10.1016/j.scitotenv.2020.140619>
- Ma, L., Wang, W.X. 2023. Dissolved rare earth elements in the Pearl River Delta: Using Gd as a tracer of anthropogenic activity from river towards the sea. *Sci. Tot. Envir.*, 856, 159241, <http://dx.doi.org/10.1016/j.scitotenv.2022.159241>.
- Möller, P., Paces, T., Dulski, P., Morteani, G., 2002. Anthropogenic Gd in surface water, drainage system, and the water supply of the city of Prague, Czech Republic. *Environ. Sci. Technol.* 36, 2387-2394. <https://doi.org/10.1021/es010235q>
- Möller, P., Morteani, G., Dulski, P. 2003. Anomalous gadolinium, cerium, and yttrium contents in the Adige and Isarco river waters and in the water of their tributaries (provinces Trento and Bolzano/Bozen, NE Italy). *Acta Hydrochim. Hydrobiol.* 31, 3, 225–239. <https://doi.org/10.1002/aheh.200300492>
- Morteani, G., Moller, P., Fuganti, A., Paces, T., 2006. Input and fate of anthropogenic estrogens and gadolinium in surface water and sewage plants in the hydrological basin of Prague (Czech Republic). *Environ. Geochem. Health* 28, 257–264. <https://doi.org/10.1007/s10653-006-9040-6>
- Nozaki, Y., Lerche, D., Alibo, D.S., Tsutsumi, M., 2000. Dissolved indium and rare earth elements in three Japanese rivers and Tokyo Bay: Evidence for anthropogenic Gd and In. *Geochim. Cosmochim. Acta* 64, 3975–3982.
- Ogata, T., Terakado, Y., 2006. Rare earth element abundances in some seawaters and related river waters from the Osaka Bay area, Japan: Significance of anthropogenic Gd. *Geochem. J.*, 40, 463-474. <https://doi.org/10.2343/geochemj.40.463>
- Petelet-Giraud, E., Klaver, G., Negrel, P., 2009. Natural versus anthropogenic sources in the surface- and groundwater dissolved load of the Dommel river (Meuse basin): constraints

by boron and strontium isotopes and gadolinium anomaly. *J. Hydrol.* 369, 336–349. <http://doi.org/10.1016/j.jhydrol.2009.02.029>

Rabiet, M., Brissaud, F., Seidel, J.L., Pistre, S., Elbaz-Poulichet, F., 2009. Positive gadolinium anomalies in wastewater treatment plant effluents and aquatic environment in the Hérault watershed (South France). *Chemosphere* 75, 1057–1064. <https://doi.org/10.1016/j.chemosphere.2009.01.036>

Song, H., Shin, W.J., Ryu, J.S., Shin, H.S., Chung, H., Lee, K.S., 2017. Anthropogenic rare earth elements and their spatial distributions in the Han River, South Korea. *Chemosphere*, 172, 155-165. <https://doi.org/http://dx.doi.org/10.1016/j.chemosphere.2016.12.135>

Zabrecky, J.M., Liu, X.-M., Wu, Q., Cao, C. 2021. Evidence of anthropogenic Gadolinium in Triangle Area Waters, North Carolina, USA. *Water*, 13, 1895. <https://doi.org/10.3390/w13141895>

Zhang, C., Wang, L., Zhang, S. 1998. Geochemistry of rare earth elements in the mainstream of the Yangtze River, China. *Appl. Geochem.*, 13, 451-462. [https://doi.org/10.1016/S0883-2927\(97\)00079-6](https://doi.org/10.1016/S0883-2927(97)00079-6)

Zhang, J., Wang, Z., Wu, Q., An, Y., Jia, H., Shen, Y. 2019. Anthropogenic Rare Earth Elements: Gadolinium in a small catchment in Guizhou Province, Southwest China. *Int. J. Environ. Res. Public Health* 16, 4052. <https://doi.org/10.3390/ijerph16204052>

Table S2: Sampling stations along the Danube

	ID	Longitude	Latitude	Danube rkm	Name
Breg	Be1	8.15483	48.09538	2819.6	Breg Source
	Be2	8.17937	48.08520	2818	Martinskapelle
	Be3	8.20636	48.05323	2813	Furtwangen
	Be4	8.30154	48.04515	2806	Voehrenbach
	Be5	8.32877	47.99747	2799	Hammereisenbach
				≈ 2799	Eisenbach – Breg junction
	Be6	8.42793	47.96790	2790	Wolterdingen
	8.48874	47.92304	2789	Huefingen	
Brigach	Bi1	8.28136	48.10704	2814.5	Brigach Source
	Bi2	8.30853	48.11446	2812.5	Brigach
	Bi3	8.39162	48.11983	2807.5	Pfaffenhof
	Bi4	8.36169	48.13059	2804.5	St-Georgen
	Bi5	8.46080	48.06305	2795	Villingen
	Bi6	8.46632	48.03342	2791	Marbach
	Bi7	8.47081	47.98236	2784	Grünigen
	Bi8	8.50058	47.95098	2778	Donaueschingen
Danube	D1	8.55001	47.93893	2772	Pfohren
	D2	8.61356	47.91583	2764	Gutmadingen
	D3	8.76209	47.95556	2747	Mohringen
	D4	8.85721	48.00725	2736	Nendingen
	D5	8.96752	48.05428	2714	Beuron
	D6	9.10008	48.08969	2698	Thiergarten
	D7	9.14048	48.07907	2692	Dietfurth
	D8	9.19428	48.07629	2686	Laiz
	D9	9.29549	48.07353	2672	Scheer
	D10	9.40077	48.07359	2662	Beuren
	D11	9.50117	48.20259	2643	Zell
	D12	9.54718	48.24043	2633	Rechtenstein
	D13	9.64159	48.23181	2623	Algershofen
	D14	9.69128	48.23227	2617	Rottenacker
	D15	9.80272	48.28494	2606	Oepffingen
	D16	9.84796	48.29665	2602	Ersingen
	D17	9.93914	48.34224	2593	Goegglingen
				≈ 2590	Iller-Danube junction
	D18	9.98659	48.39005	2588	Ulm
	SW1-D	10.02804	48.42501	2581	Boefinger Halede
	SW2-D	11.15505	48.73665	2479	Bittenbrunn
	SW3-D	11.86573	48.91761	2415	Kelheim
	SW4-D	13.01017	48.77495	2276	Niederalteich
			2225	Inn – Danube junction	
SW6-D	13.70383	48.52164	2204	Jochenstein	
SW7-D	14.51204	48.24042	2213	Enghagen	

SW8-D	15.53335	48.38427	2008	Oberloihen
SW9-D	16.32987	48.33012	1942	Klosterneuburg
SW10-D	16.95265	48.16498	1879	Hainburg
			≈ 1869	Morava – Danube junction
SW14-D	17.08400	48.14000	1868	Bratislava
SW15-D	17.23058	48.04025	1855	Čunovo
SW16-D	17.65977	47.78952	1806	Medvedov
			≈ 1794	Moson Danube arm
SW18-D	17.84397	47.74265	1790	Gönyü
			≈ 1766	Váh – Danube junction
			≈ 1716	Hron – Danube junction
			≈ 1708	Ipel – Danube junction
SW22-D	18.86323	47.81340	1707	Szob
SW23-D	19.19177	47.61603	1660	Budapest-Megyeri Bridge
SW24-D	19.00408	47.38830	1630	Budapest-MO Bridge
			≈ 1586	Ráckevei-Soroksári Danube branch
SW26-D	18.92632	46.81707	1560	Dunafoldvar
SW27-D	18.88042	46.63373	1532	Paks
SW28-D	18.92350	46.20053	1481	Baja
SW29-D	18.80593	45.91455	1434	Hercegszanto
			≈ 1382	Drava – Danube junction
SW31-D	19.36060	45.23158	1300	Ilok
			≈ 1214	Tisza – Danube junction
			≈ 1170	Sava – Danube junction
SW37-D	20.64443	44.81447	1151	Pancevo
			≈ 1103	Velika Morava – Danube junction
SW40-D	21.38380	44.80510	1073	Banatska_Palanka
SW41-D	22.68498	44.26092	847	Timok
			≈ 846	Timok – Danube junction
SW43-D	22.78217	44.17230	837	Pristol
			≈ 636	Iskar – Danube junction
			≈ 537	Jantra – Danube junction
			≈ 498	Rusenski Lom – Danube junction
SW47-D	26.06696	43.91083	488	Ruse
SW48-D	27.05112	44.13693	375	Chiciu
			≈ 133	Prut – Danube junction
SW50-D	28.26013	45.45630	132	Reni
SW51-D	29.58140	45.39455	18	Vilkova

Table S3: Sampling stations along the Danube tributaries

ID	Longitude	Latitude	Rkm to junction	Name	DOC (mgC/L)	Nitrates (mg/L)
E1	8.32908	47.99694	0.5	Eisenbach	1.51	1.87
I1	9.98839	48.37078	0.5	Iller	1.33	5.75
SW5-Inn	13.43713	48.55670	4	Inn	0.49	2.03
SW11-Mor	16.88528	48.72349	17	Thaya – Morava junction	7.52	4.87
SW12-Mor	16.98931	48.68721	79	Landzhot/Morava	4.53	4.23
SW13-Mor	16.97596	48.18768	1	Devin/Morava	4.94	4.14
SW17-Mos	17.78158	47.73617	0.1	Venek/Moson	2.71	5.00
SW19-Vah	18.14233	47.76091	1.5	Komarno/Vah	3.39	3.44
SW20-Hron	18.72334	47.82608	1.7	Kamenica/Hron	2.84	6.26
SW21-Ipel	18.76256	47.88596	12	Salka/Ipel	5.60	3.33
SW25-Rac	18.97820	47.03398	59	Tass/Rackevei-Soroksari	2.29	2.63
SW30-Drav	18.86460	45.55224	5	Drava	1.45	2.42
SW32-Tis	20.10467	46.18552	163	Tiszasziget/Tisza	3.46	2.62
SW33-Tis	20.28087	45.14700	1	Tisza mouth	4.11	4.13
SW34-Sava	15.69200	45.86092	729	Jesenice_na_Dolenjskem/Sava	2.24	5.58
SW35-Sava	19.08364	44.87828	205	Jamena/Sava	2.85	3.34
SW36-Sava	20.39607	44.79300	7	Sava mouth	2.96	2.73
SW38-Vel	21.38000	43.74000	154	Varvarin/Velika_Morava	2.35	3.08
SW29-Vel	21.03570	44.70927	1	Velika_Morava mouth	3.59	0
SW42-Timok	22.67215	44.21492	0.2	Timok mouth	1.59	5.94
SW44-Iskar	24.44382	43.72990	0.3	Iskar mouth	3.00	8.00
SW45-Jan	25.56987	43.63748	1	Jantra mouth	4.55	7.17
SW46-Rus	25.93092	43.83482	0	Rusenki Lom mouth	4.07	29.7
SW49-Prut	28.19673	45.47187	0.5	Giurgiulesti/Prut	6.74	0.47

Table S4: Test of the SLRS-6 reference material: % error of our measurements with respect to the reference values

	Reference value (ng/L) (Yeghicheyan et al., 2019)	% Error
La	248.3	0.86
Ce	292.7	0.05
Pr	59.1	0.55
Nd	227.8	1.15
Sm	39.5	1.86
Eu	7.26	7.07
Gd	31.6	2.37
Tb	4.07	16.13
Dy	21.9	3.97
Ho	4.3	6.13
Er	12.4	5.46
Tm	1.79	0.79
Yb	11.2	2.39
Lu	1.91	2.72

Table S5 : Coding of the main geological characteristics of the Danube watershed upstream of Ulm

Code	Stratigraphy	Main rocks
pz-plu	Upper Proterozoic - Upper Paleozoic	Orthogneiss, granite
so	Triassic, Upper Buntsandstein	Sandstone
cs	Upper Carboniferous to Rotliegend	Granite Sandstone, Conglomerate
m	Triassic, Muschelkalk	Limestone, marlstone,
km	Triassic, Middle Keuper	Marlstone
ju	Jurassic, Lower Jurassic (Lias)	Marlstone

jm	Jurassic, Middle Jurassic (Dogger)	Marlstone
jo	Jurassic, Upper Jurassic (Malm)	Marlstone, limestone
qR	Rift cold period	Gravel and sand, partly stony
qh	Holocene	Peat
tUSM	Tertiary, Lower Freshwater Molasse	Sandstone

Table S6 : Main ions concentrations in the Danube tributaries during JDS4

	Sulfates (mg/L)	Chlorides (mg/L)	Sodium (mg/L)	Magnesium (mg/L)	Calcium (mg/L)	Potassium (mg/L)
JDS4-5 Inn rkm 4	17.7	4.6	0.3	0.7	2.9	0.2
JDS4-11 Morava/Dyje rkm 17	92.2	56.2	4.0	2.0	5.9	1.0
JDS4-13 Morava rkm 1	68.8	39.6	2.8	1.5	6.1	0.8
JDS4-19 Vah rkm 1.5	34.2	19.1	12.7	14.0	52.7	3.4
JDS4-20 Hron rkm 1.7	51.4	22.3	18.1	19.2	58.8	4.8
JDS4-21 Ipel rkm 12	59.7	35.0	39.8	36.7	105.2	15.7
JDS4-25 Ráckevei-Soroksári rkm 59	24.9	15.0	9.2	11.3	41.4	2.8
JDS4-30 Drava rkm 5	20.5	7.4	5.1	8.7	38.0	2.3
JDS4-33 Tisza rkm 1	33.8	33.1	21.9	9.1	41.9	3.8
JDS4-36 Sava rkm 7	19.1	22.5	7.4	10.9	59.6	1.9
JDS4-38 Velika Morava rkm 154	26.4	10.5	8.5	18.2	37.6	2.5
JDS4-39 Velika Morava rkm 1	30.7	12.1	10.2	17.3	21.2	2.9
JDS4-42 Timok rkm 0.2	221.4	10.9	12.2	19.8	128.4	2.9
JDS4-44 Iskar rkm 0.3	38.6	16.8	13.5	12.0	48.6	3.5
JDS4-45 Jantra rkm 1	27.3	9.5	11.3	12.3	61.3	3.3
JDS4-46 Russenski Lom rkm 0	38.0	25.5	23.5	38.4	83.0	6.5
JDS4-49 Prut rkm 0.5	82.9	21.5	33.2	16.2	56.6	6.6

a)	b)
----	----

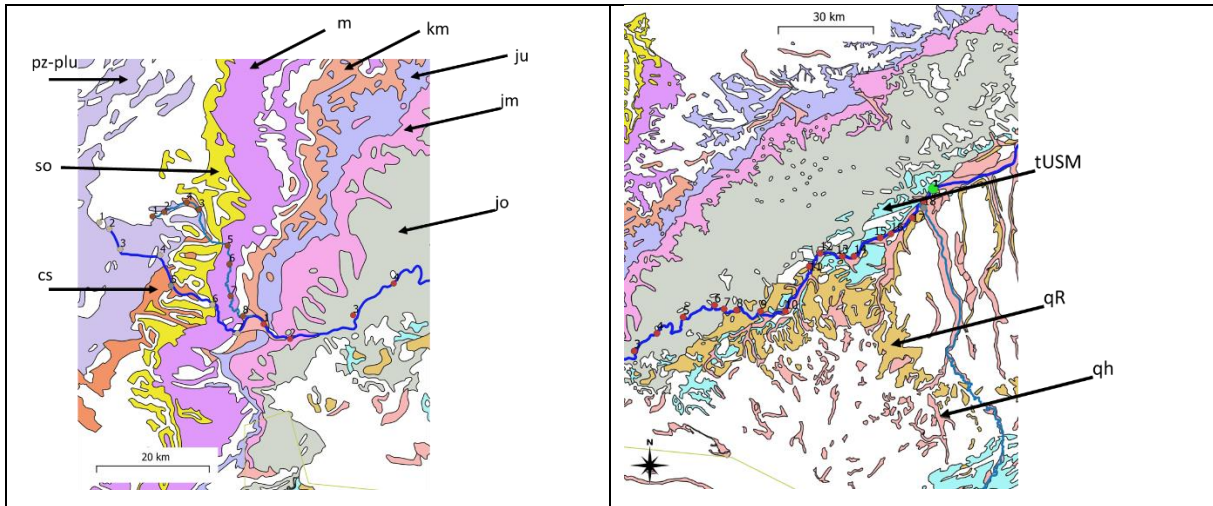
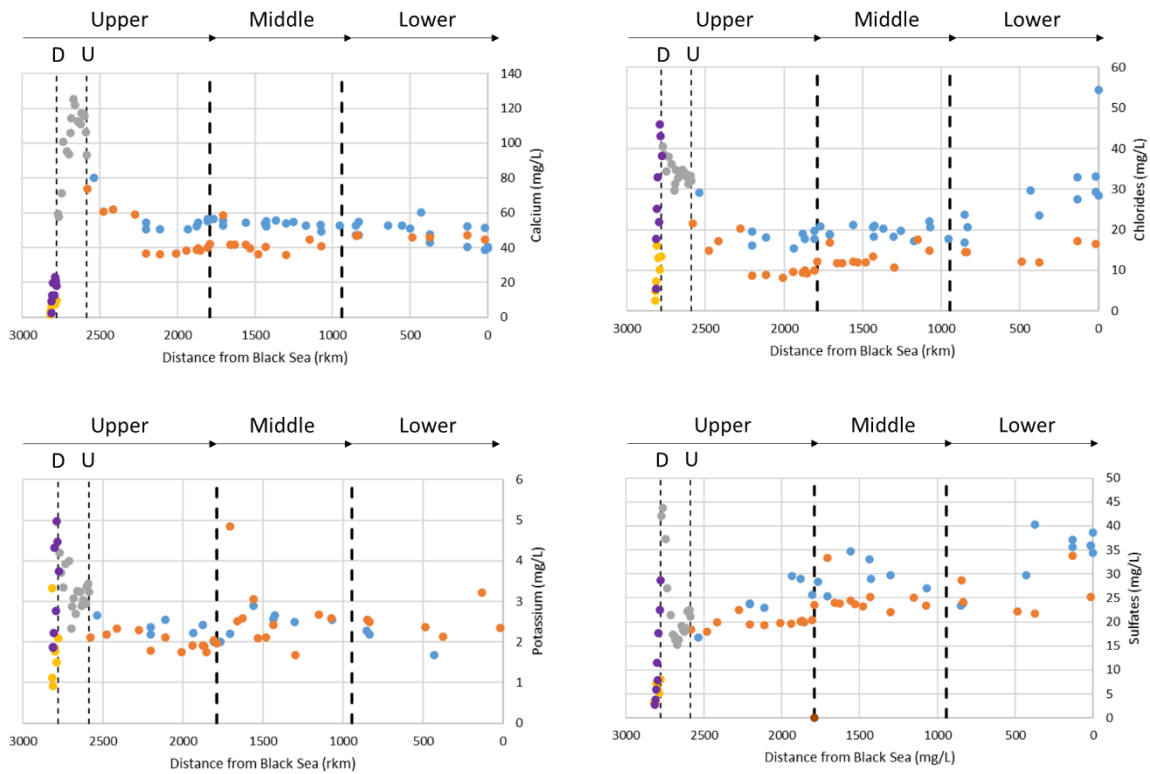


Figure S1: Main geological characteristics a) between the sources and Nendingen (Germany) b) between Mohringen (Germany) and Ulm. Codes in Table SI4.



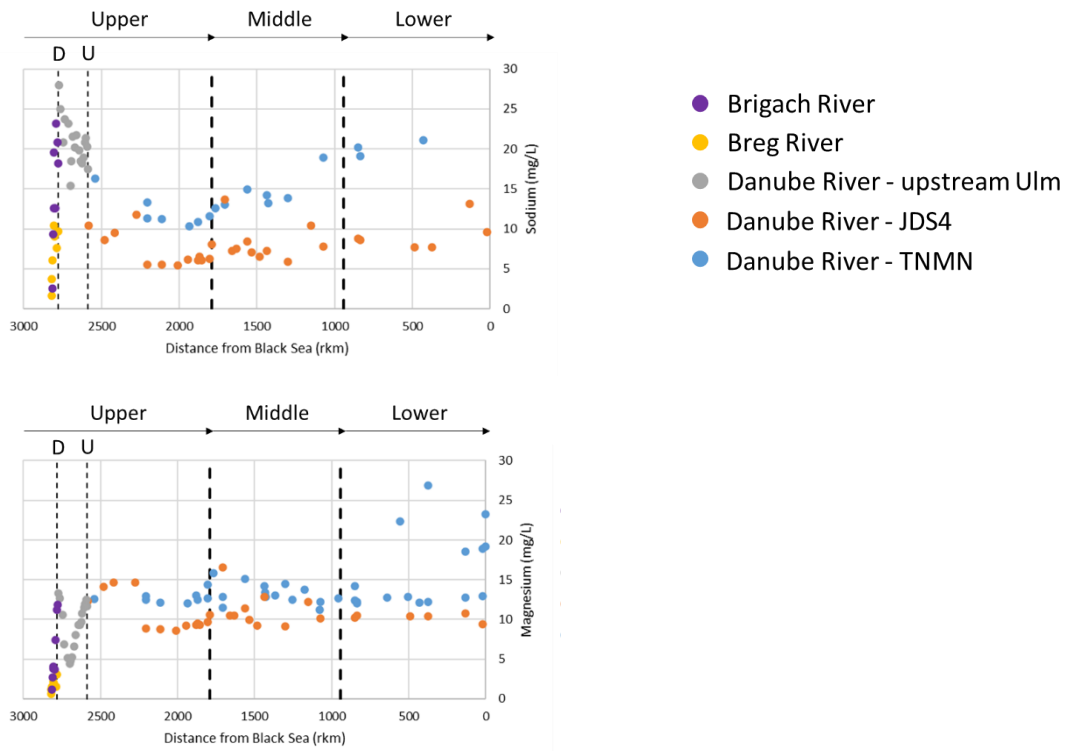


Figure S2: Main anions concentrations along the Danube River during JDS4. Comparison with the TNMN data for 2017. Donaueschingen = D, Ulm = U

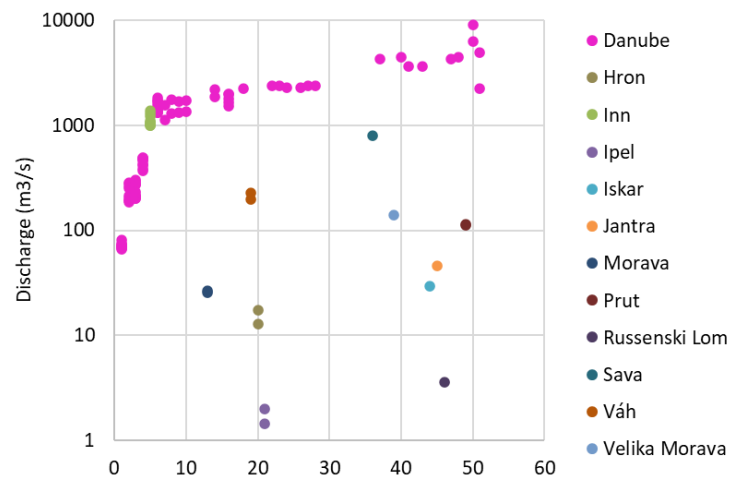


Figure S3: Discharge of the Danube River and its main tributaries during the sampling period (July 2019)

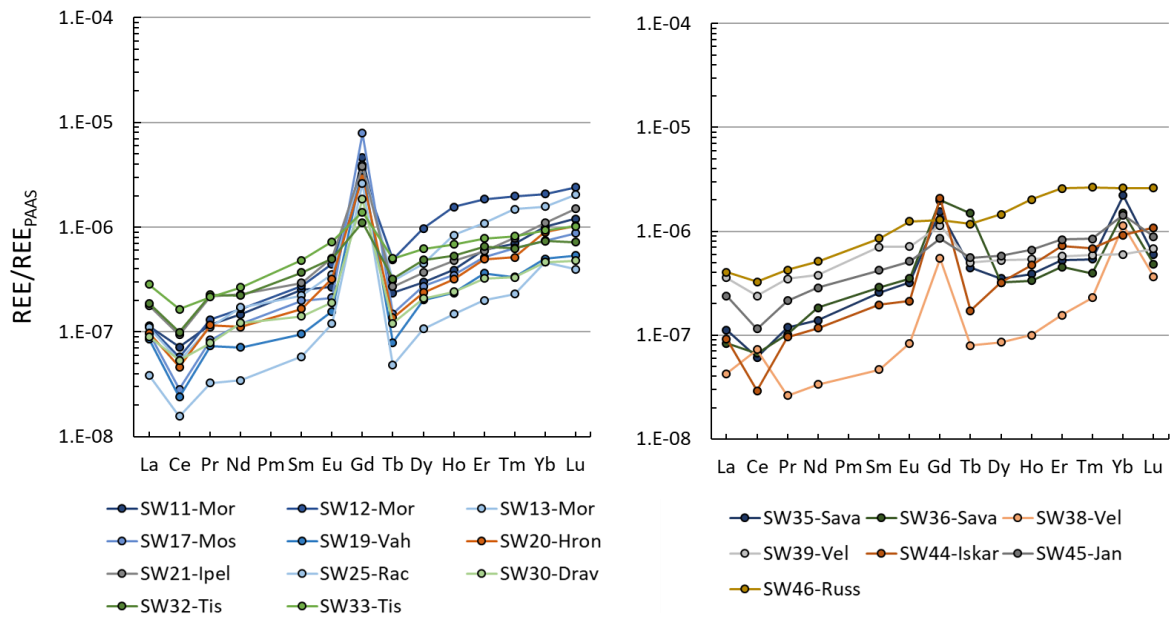


Figure S4: REE patterns, normalized with respect to PAAS, on Danube River tributaries

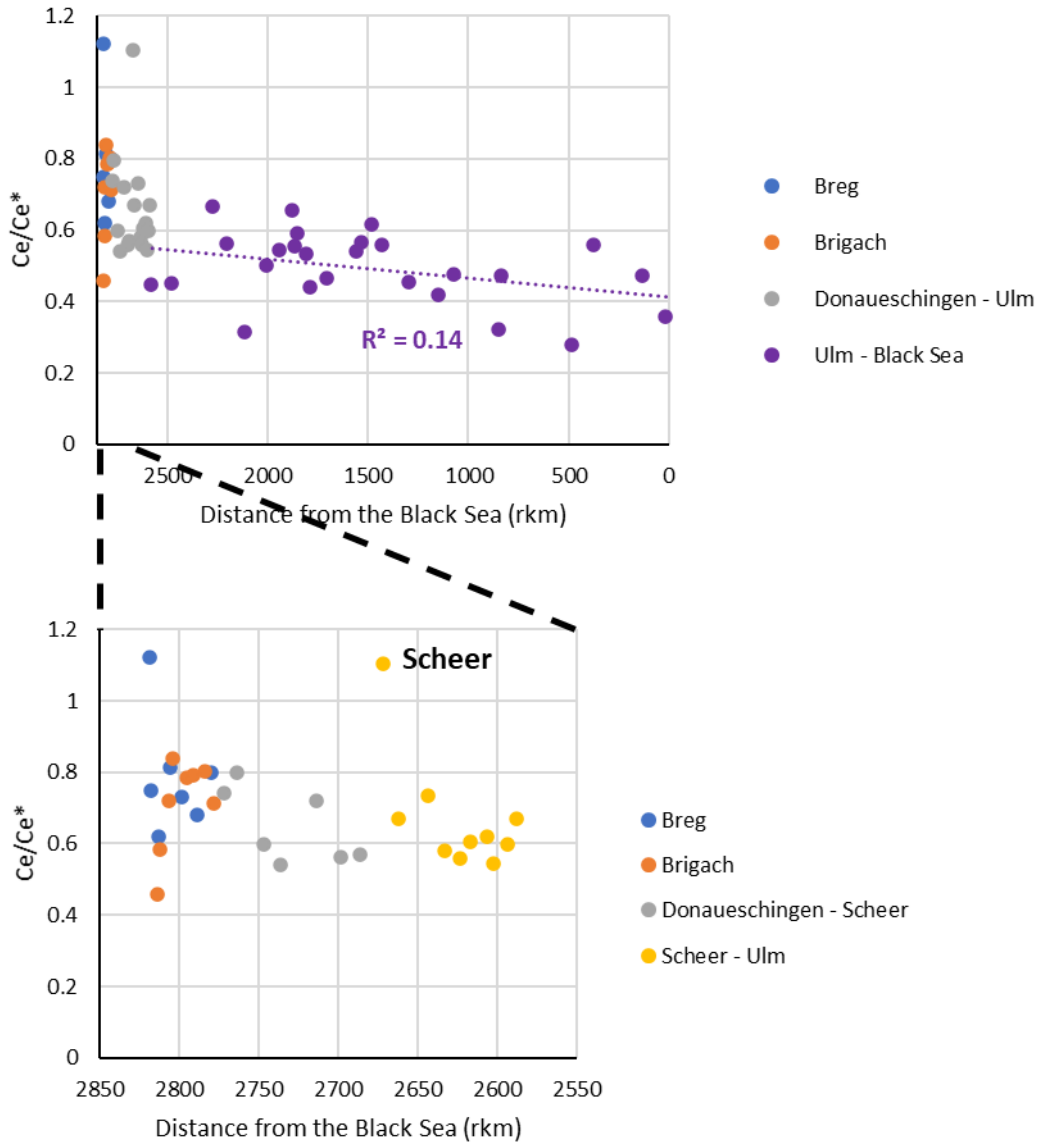


Figure S5: Cerium anomaly (Ce/Ce*) along the Danube River

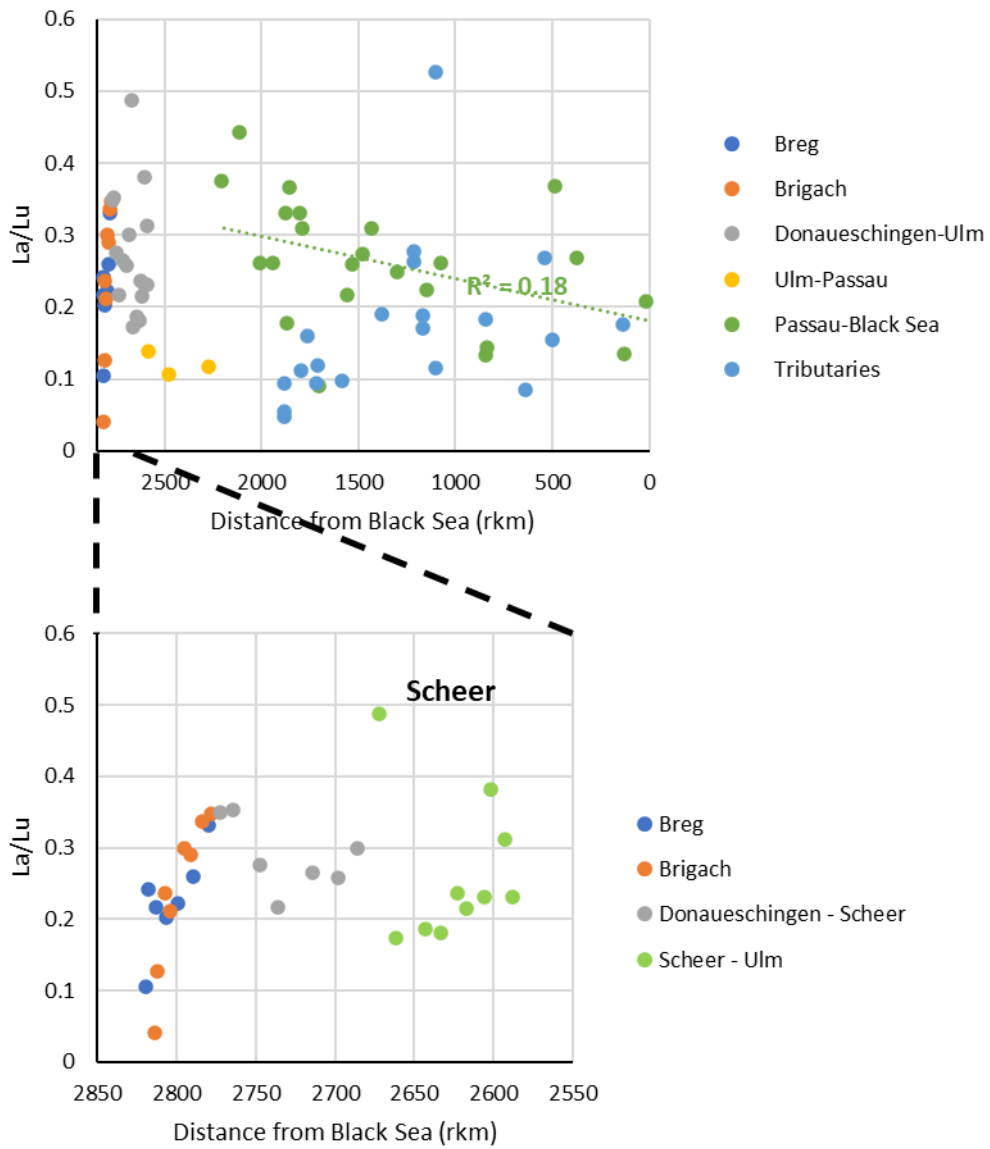


Figure S6: La/Lu along the Danube River and its tributaries

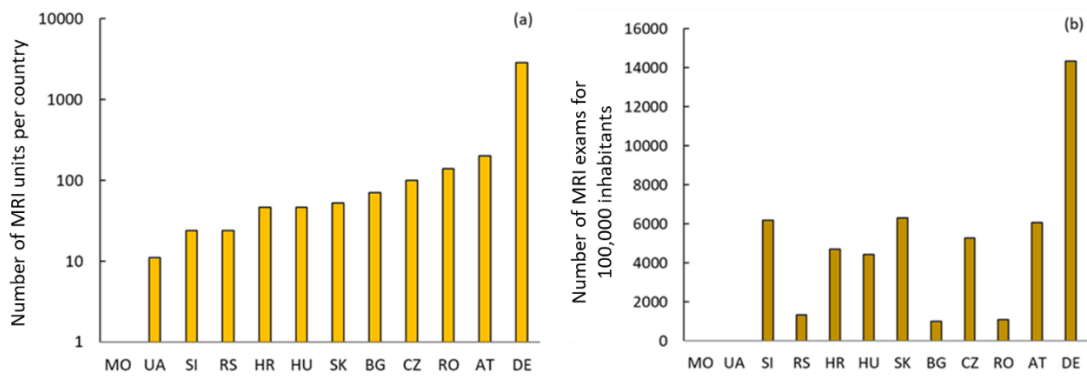


Figure S7: Number of MRI units per country (a) and number of MRI exams per 100,000 inhabitants (b) in the Danube River watershed

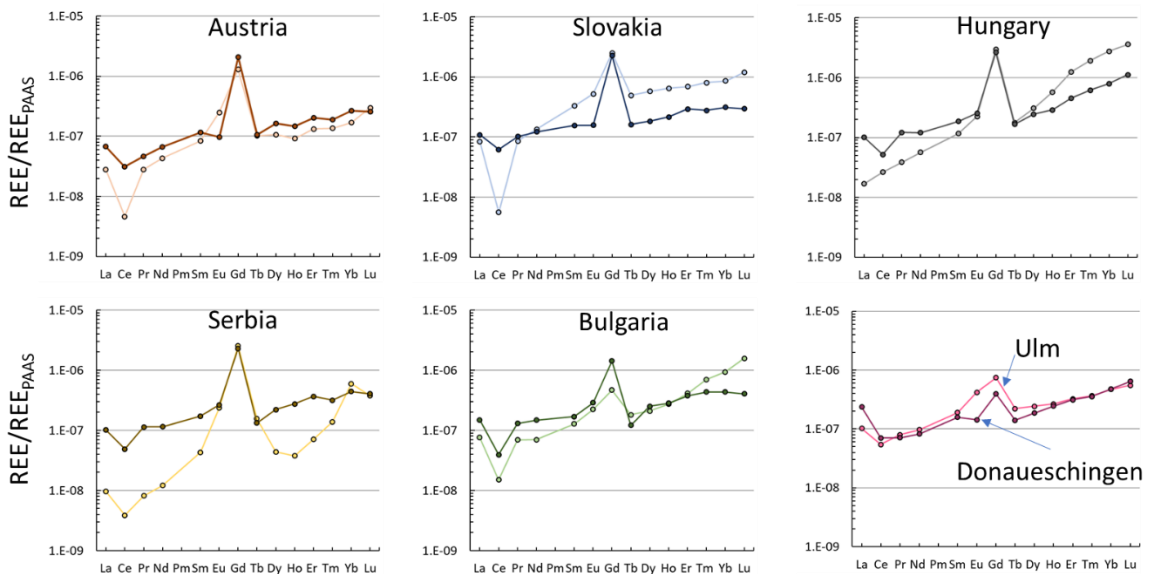


Figure S8: REE patterns of groundwater samples (open symbols) and their closest Danube River JDS4 station (closed symbols) (SW9-D for Austria, SW15-D for Slovakia, SW22-D for Hungary, SW31-D for Serbia and SW47 for Bulgaria) and of tapwater in Ulm and Donaueschingen

